



RESEARCH ARTICLE

10.1002/2017GC007227

Tracking Formation of a Lava Lake From Ground and Space: Masaya Volcano (Nicaragua), 2014–2017

Special Section:

Carbon Degassing Through Volcanoes and Active Tectonic Regions

Alessandro Aiuppa^{1,2} , J. Maarten de Moor³ , Santiago Arellano⁴ , Diego Coppola⁵ , Vincenzo Francofonte², Bo Galle⁴, Gaetano Giudice² , Marco Liuzzo² , Elvis Mendoza⁶, Armando Saballos⁶, Giancarlo Tamburello^{1,7} , Angelo Battaglia¹ , Marcello Bitetto¹ , Sergio Gurrieri² , Marco Laiolo⁸, Andrea Mastroli², and Roberto Moretti⁹

Key Points:

- We present a multidisciplinary study of the formation mechanisms of a lava lake at Masaya (Nicaragua), December 2015
- We find evidence for a gas CO₂/SO₂ ratio precursor prior to (re)formation of the Masaya lava lake
- We interpret formation of the lava lake as driven by elevated supply of deeply sourced CO₂-rich gas bubbles

Supporting Information:

- Supporting Information S1
- Table S1

Correspondence to:

A. Aiuppa,
alessandro.aiuppa@unipa.it

Citation:

Aiuppa, A., de Moor, J. M., Arellano, S., Coppola, D., Francofonte, V., Galle, B., . . . Moretti, R. (2018). Tracking formation of a lava lake from ground and space: Masaya volcano (Nicaragua), 2014–2017. *Geochemistry, Geophysics, Geosystems*, 19, 496–515. <https://doi.org/10.1002/2017GC007227>

Received 12 SEP 2017

Accepted 11 JAN 2018

Accepted article online 22 FEB 2018

Published online 27 FEB 2018

¹Dipartimento DiSTeM, Università di Palermo, Palermo, Italy, ²Istituto Nazionale di Geofisica e Vulcanologia, Sezione di Palermo, Palermo, Italy, ³Observatorio Vulcanológico y Sismológico de Costa Rica, Universidad Nacional, Heredia, Costa Rica, ⁴Chalmers University of Technology, Department of Space, Earth and Environment, Microwave and Optical Remote Sensing, Gothenburg, Sweden, ⁵Dipartimento di Scienze della Terra, Università di Torino, Torino, Italy, ⁶Dirección de Vulcanología, Instituto Nicaraguense De Estudios Territoriales (INETER), Managua, Nicaragua, ⁷Istituto Nazionale di Geofisica e Vulcanologia, Sezione di Bologna, Bologna, Italy, ⁸Dipartimento di Scienze della Terra, Università di Firenze, Firenze, Italy, ⁹Dipartimento di Ingegneria Civile Design, Edilizia e Ambiente Seconda Università degli Studi di Napoli, Naples, Italy

Abstract A vigorously degassing lava lake appeared inside the Santiago pit crater of Masaya volcano (Nicaragua) in December 2015, after years of degassing with no (or minor) incandescence. Here we present an unprecedented-long (3 years) and continuous volcanic gas record that instrumentally characterizes the (re)activation of the lava lake. Our results show that, before appearance of the lake, the volcanic gas plume composition became unusually CO₂ rich, as testified by high CO₂/SO₂ ratios (mean: 12.2 ± 6.3) and low H₂O/CO₂ ratios (mean: 2.3 ± 1.3). The volcanic CO₂ flux also peaked in November 2015 (mean: 81.3 ± 40.6 kg/s; maximum: 247 kg/s). Using results of magma degassing models and budgets, we interpret this elevated CO₂ degassing as sourced by degassing of a volatile-rich fast-overturning (3.6–5.2 m³ s⁻¹) magma, supplying CO₂-rich gas bubbles from minimum equivalent depths of 0.36–1.4 km. We propose this elevated gas bubble supply destabilized the shallow (<1 km) Masaya magma reservoir, leading to upward migration of vesicular (buoyant) resident magma, and ultimately to (re)formation of the lava lake. At onset of lava lake activity on 11 December 2015 (constrained by satellite-based MODIS thermal observations), the gas emissions transitioned to more SO₂-rich composition, and the SO₂ flux increased by a factor ~40% (11.4 ± 5.2 kg/s) relative to background degassing (8.0 kg/s), confirming faster than normal (4.4 versus ~3 m³ s⁻¹) shallow magma convection. Based on thermal energy records, we estimate that only ~0.8 of the 4.4 m³ s⁻¹ of magma actually reached the surface to manifest into a convecting lava lake, suggesting inefficient transport of magma in the near-surface plumbing system.

1. Introduction

Emergence of a new lava lake is a relatively rare and exceptional event in Nature. Stable, nearly persistent lava lakes are scarce volcanic features on Earth, existing at Ambrym volcano in Vanuatu (Allard et al., 2015), Erebus in Antarctica (Oppenheimer et al., 2009), Erta Ale in Ethiopia (Vergnolle & Bouche, 2016), Nyiragongo in Congo (Burgi et al., 2014), and Villarrica in Chile (Palma et al., 2008). Formation or rebirth of lava lakes is even less frequently observed. Recent examples of lava lake emergence include Halema'uma'u Crater on Kilauea in 2008 to present (Patrick et al., 2013, 2016) and Nyamuragira in 2012–2014 (Coppola et al., 2016a). The processes leading to (re)formation of a lava lake are not well understood due to the limited observations available.

Masaya volcano (Figure 1) in Nicaragua has nearly continuous historical record of magma appearing and disappearing in the crater floor since the time of the first sightings by the Spanish conquistadors in 1524–1529 (Global Volcanism Program, 2013; Rymer et al., 1998). Since its formation in 1858–1859 (McBirney, 1956), Masaya's Santiago pit crater (Figure 1) has intermittently hosted one or more incandescence vents of variable size and degassing activity (Rymer et al., 1998). Occasionally, these vents have enlarged in dimension, most likely due to magma level increase in the conduit and crater floor collapse, ultimately leading to

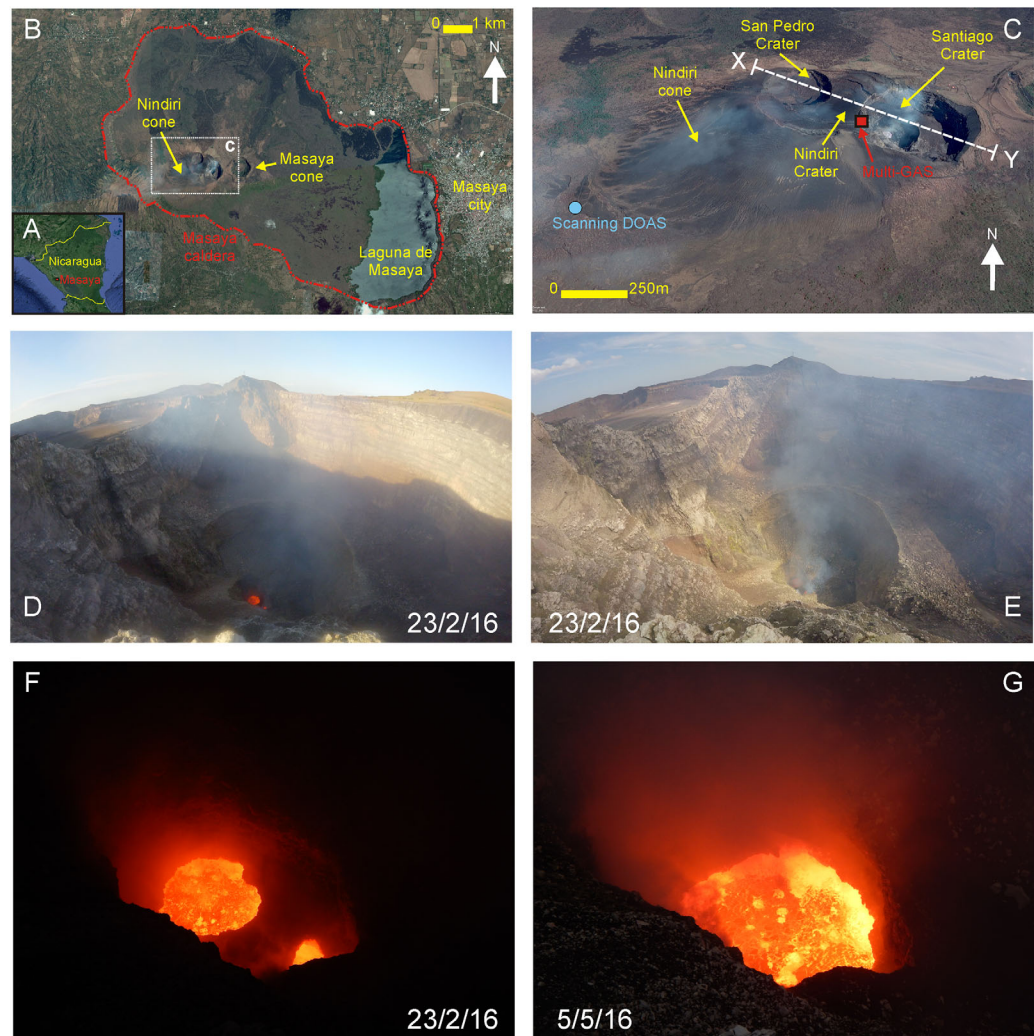


Figure 1. (a) Google Earth map showing location of Masaya volcano in Nicaragua; (b) the Masaya caldera (red dotted line), with the Masaya and Nindiri cones in its center; (c) a zoom of the Nindiri cone (see white box in Figure 1b for location), showing the active Santiago pit crater along with the currently quiescent Nindiri and San Pedro craters. Locations of the DECADE Multi-GAS and the scanning NOVAC spectrometer are also shown; (d, e) panoramic views of the inner Santiago crater, taken on 23 February 2016, with the active lava lake visible on the crater bottom; (f) night view of the Santiago crater floor on 23 February 2016, showing two distinct lakes; (g) night view of the Santiago crater floor on 5 May 2016. The two to three lava lakes formed during December 2015 to February 2016 had merged into a single, vigorously active lake.

formation of an “active lava lake.” Such a lava lake formation events in the Santiago crater floor have typically been associated with strong degassing episodes, each lasting years to decades (Delmelle et al., 1999; Stoiber et al., 1986), making Masaya one of the strongest degassing sources in the Central America Volcanic Arc (Aiuppa et al., 2014; Martin et al., 2010; Mather et al., 2006).

The latest Santiago degassing crisis started in 1993 and has persisted with fluctuating vigor until present (Delmelle et al., 1999; Stix, 2007; Williams-Jones et al., 2003). Although little or no magma has been erupted out of the crater, voluminous amounts of magmatic gas have been vented into the atmosphere (Burton et al., 2000; de Moor et al., 2013; Horrocks, 2001; Martin et al., 2010; Moune et al., 2010; Nadeau & Williams-Jones, 2009; Stoiber et al., 1986), resulting in substantial environmental impact on the surroundings and local communities (Delmelle et al., 1999, 2002). This unusually persistent degassing activity has also motivated extensive geophysical work in the attempt to resolve the structure of the shallow plumbing system (Delmelle et al., 1999; Rymer et al., 1998; Williams-Jones et al., 2003), and the magma circulation pathways/rates therein (Stix, 2007). Based on results of periodic gravity surveys, Rymer et al. (1998) and Williams-Jones

et al. (2003) proposed that the Masaya cyclic degassing crises are caused by convective replacement of dense, degassed magma by gas-rich vesicular magma in the shallow (<1 km depth) plumbing system. These authors also argued such convective overturning is not necessarily triggered by intrusion of fresh (gas-rich) magma but may simply be initiated by degassing/crystallization (and consequent sinking) of shallow resident magma. However, volcanic gas information has never been available for the onset of a degassing crisis to test the likelihood of the two possible scenarios, i.e., intrusion of fresh magma versus convection of resident magma.

A vigorously degassing, actively convecting lava lake formed in the Santiago crater between December 2015 and March 2016, marking the end of a 3 yearlong period of reduced activity and the onset of a new period of elevated degassing. Before, during, and after formation of the lava lake, the composition and flux of volcanic gases were systematically measured using a permanent gas network that includes a Multi-Component Gas Analyzer System (Multi-GAS; Aiuppa et al., 2005) of the DECADE network and a scanning-Differential Optical Absorption Spectrometer (DOAS) of the NOVAC (Network for Observation of Volcanic and Atmospheric Change) network (Galle et al., 2010). At the same time, infrared images acquired by the Moderate Resolution Imaging Spectroradiometer (MODIS), elaborated by the Middle Infrared Observation of Volcanic Activity (MIR-OVA) system (Coppola et al., 2016b), were used to detect and quantify thermal anomalies related to the lava lake activity inside Santiago crater. Thanks to integration of these ground-based and satellite-based data, transition to a lava lake phase was observed for the first time, yielding novel information on the underlying driving processes. Summarizing the key observations obtained, and their implications for our knowledge of the volcano's degassing mechanisms and behavior, is the objective of the present study.

2. Materials and Methods

2.1. Masaya Volcano

Masaya is a tholeiitic basaltic shield volcanic complex (Walker et al., 1993) in Central Nicaragua (Figure 1a), world-renown for its nearly persistent open-vent degassing activity (Stix, 2007) and for having produced some of the few examples of basaltic plinian eruptions (Kutterolf et al., 2007; Pérez et al., 2009; van Wyk de Vries, 1993; Williams, 1983). The Masaya volcano in a strict sense is the youngest shield edifice of the complex and sits on an older sequence of nested calderas and craters. Masaya is cut on its summit by a NW-SE elongated caldera that is 11 km long by 6 km wide (Figure 1b) and was formed by at least three major (plinian) basaltic eruptions between ~6 and 1.8 ka ago (Bice, 1985; Kutterolf et al., 2007, 2008; Pérez et al., 2009; Pérez & Freundt, 2006; van Wyk de Vries, 1993; Williams, 1983). The post 1.8 ka activity has been concentrated in the caldera center along a semicircular set of vents/cones, today topped by four pit craters, among which is the currently active Santiago crater (Rymer et al., 1998; Figure 1c).

The Santiago pit crater (Figures 1d and 1e) formed in a sequence of collapse/explosion events in 1858–1859 (McBirney, 1956; Rymer et al., 1998) and has since remained the main site of activity at Masaya. During its short-lived history, Santiago has alternated between (i) periods of intense degassing associated with opening of active vents on the crater floor eventually culminating with lava lake formation (such as in 1965–1969, 1972–1979, 1989, and 1993–1994) and (ii) phases of reduced activity. Each “degassing crisis” has typically lasted years to decades (the most recent started in 1993) and has typically fluctuated between vent-opening phases (mostly due to unroofing of small chambers beneath the crater floor) and vent-closing phases (due to rockfalls inside the crater; Rymer et al., 1998). Occasionally, the latter crater wall collapse events have been followed by vent-clearing ash explosions, such as in 2001 (Duffell et al., 2003) and in April–May 2012 (Global Volcanism Program, 2016; Pearson et al., 2012). After a period of reduced volcanic activity between late 2012 and late 2015, incandescence was again reported on the crater floor by INETER on 11 December 2015 (Global Volcanism Program, 2016). Between mid-December 2015 and March 2016, two to three incandescent vents (Figure 1f) became visible, which progressively widened to merge into a single, vigorously active lava lake (Figure 1g), perhaps due to collapsing of the crater floor. Intense seismicity and SO₂ degassing have been associated with formation of the lava lake (Global Volcanism Program, 2016). The lava lake is still active at the time of writing.

2.2. Gas Measurements

We field deployed a Multi-GAS on Masaya in March 2014, as part of the global network of the Deep Earth Carbon Degassing (DECADE; <https://deepcarboncycle.org/home-decade/>) project funded by the Deep

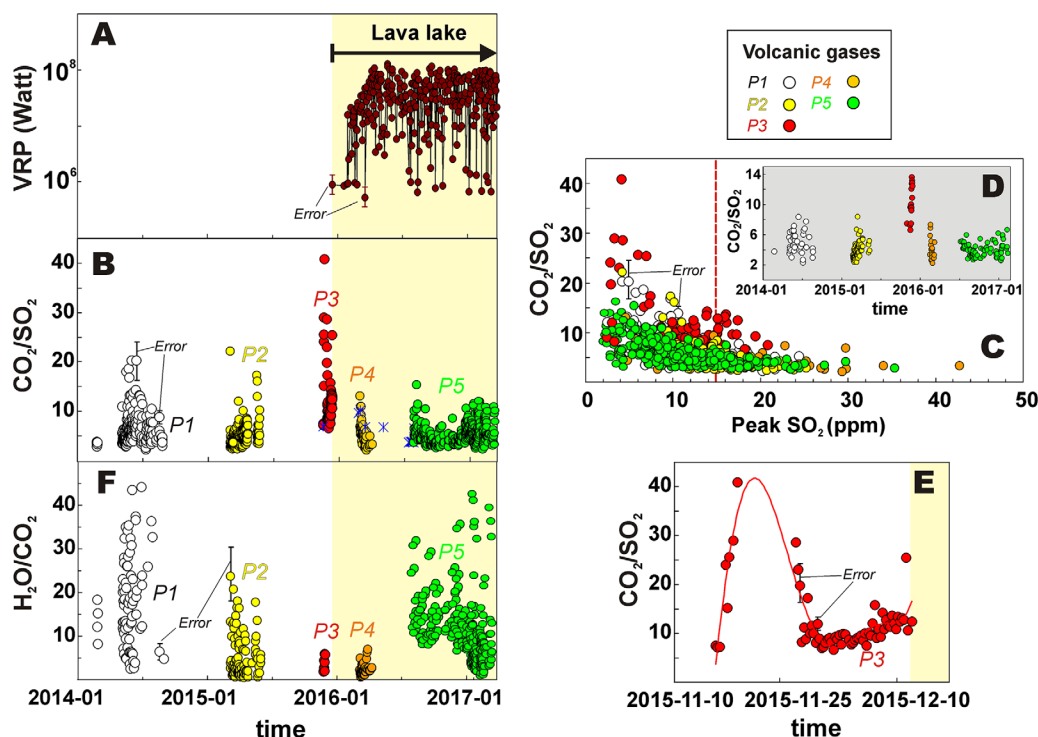


Figure 2. (a) Time series of the volcanic radiant power (VRP, in W), January 2014 to March 2017. The lake is first detected on 11 December 2015. Thermal radiance then grows from December to mid February 2016, when a plateau is reached. (b) Time series of molar CO_2/SO_2 ratios. Each point corresponds to the time-averaged CO_2/SO_2 ratio calculated in a 30 min-long Multi-GAS acquisition window (raw data and CO_2/SO_2 ratios are accessible at <https://doi.org/10.1594/IEDA/100651>). Data are divided into five subintervals (which we refer to as subintervals P1–P5), during which data acquisition was continuous. The five cycles are shown in different colors: P1, white; P2, yellow; P3, red; P4, orange; and P5, green. CO_2/SO_2 ratios are anomalously high in subinterval P3, prior to lake formation. The blue stars identify the periodic survey results reported in de Moor et al. (2017). (c) Plot of molar CO_2/SO_2 ratios versus peak SO_2 concentration (the maximum SO_2 value recorded in the corresponding 30 min-long Multi-GAS acquisition window). The five Masaya gas populations converge to relatively constant (and SO_2 -independent) CO_2/SO_2 ratios in dense plume conditions (>10 ppm peak SO_2 concentrations). (d) The CO_2/SO_2 ratio gas population (of Figure 2b) filtered using a 15 ppm SO_2 threshold. (e) Time series of the CO_2/SO_2 ratio for period P3, from 11 October to 10 December 2015. (f) Time series of molar $\text{H}_2\text{O}/\text{CO}_2$ ratios. Each point corresponds to the time-averaged $\text{H}_2\text{O}/\text{CO}_2$ ratio calculated in a 30 min-long Multi-GAS acquisition window (raw data and $\text{H}_2\text{O}/\text{CO}_2$ ratios are accessible at <https://doi.org/10.1594/IEDA/100651>). Error bars for some representative measurement points are shown.

Carbon Observatory (DCO; <https://deepcarbon.net/>). This fully autonomous gas sensing unit was installed on the outer rim of the Santiago pit crater (coordinates: $11^\circ59'14.410''\text{N}$, $-86^\circ10'3.734''\text{W}$, see Figure 1c). The Multi-GAS is still operating by November 2017, but 3 years of results (March 2014 to March 2017) are discussed here. The instrument measured in situ the mixing ratio of CO_2 , SO_2 , and H_2S in the volcanic gas plume, using the established combination of Near Dispersive Infra Red (NDIR) spectrometers and electrochemical sensors described in previous work (Aiuppa et al., 2014, 2017). Ambient pressure, temperature, and relative humidity were also comeasured, from which the in-plume H_2O mixing ratio were obtained using the Arden Buck equation (Buck, 1981). Data acquisition was controlled by a Moxa embedded computer (model 7112plus), and the whole system was powered by two batteries and a 120 W solar panel. The Multi-GAS unit was programmed to acquire data (at 0.1 Hz) during four daily measurement cycles, each 30 min long. The acquired data were stored in an onboard data logger and telemetered to the INETER base station in Managua using a radio link. Concentration data were then postprocessed using the Ratiocalc software (Tamburello, 2015) to obtain time series of the volcanic gas CO_2/SO_2 and $\text{H}_2\text{O}/\text{CO}_2$ molar ratios. The data set is accessible at (<https://doi.org/10.1594/IEDA/100651>), which lists (i) raw (mixing ratio) data and (ii) time-averaged CO_2/SO_2 and $\text{H}_2\text{O}/\text{CO}_2$ ratios for 30 min-long Multi-GAS acquisition windows. No ratio was derived for acquisition windows in which the maximum SO_2 concentration was <3 ppmv threshold and/or low correlation coefficients ($R^2 \leq 0.6$) between gas species were observed. Based on laboratory tests with

standard gases, errors in derived ratios are typically $\leq 15\%$ and $\leq 30\%$ for CO_2/SO_2 and $\text{H}_2\text{O}/\text{CO}_2$ ratios, respectively. The sensors' calibration was also regularly checked in the laboratory using calibration gases at the beginning and end of each measurement subinterval *P1–P5* (see below), and no substantial drift or change was observed.

The volcanic CO_2 flux is calculated from combination of coacquired CO_2/SO_2 ratios and SO_2 fluxes. SO_2 flux is obtained for the period March 2014 to February 2017, from evaluation of data of one scanning-DOAS station from the NOVAC network, located ~ 1.5 km WSW of Santiago crater at an altitude of 387 m asl (see Figure 1c). The instrument points to the Santiago crater and scans the plume over a flat surface from horizon to horizon, at steps of 3.6° , recording at each step spectra of solar scattered radiation in the 280–450 nm wavelength range (effective range between 300 and 360 nm due to atmospheric and optical filters). The system is a standard NOVAC-Mark I instrument, which specifications are described by Galle et al. (2010). Each scan is completed in about 5 min during daylight. By integrating the column densities of SO_2 , derived by the DOAS method (Platt & Stutz, 2008), over a cross section of the plume, and multiplying by the transport speed, the flux of SO_2 is derived. For this evaluation, we used wind speed from the ECMWF ERA-Interim database (Dee et al., 2011) with a spatial resolution of $0.125^\circ \times 0.125^\circ$ and a temporal resolution of 6 h, which was then interpolated to the coordinates of the crater and time of each measurement. Plume direction was obtained by observing the distribution of column densities on each scan, and assuming that the plume centre of mass was drifted at the summit level. Only measurements that were elevated (to ensure complete plume coverage and availability of a background spectrum for cancellation of instrumental and atmospheric effects) were used for further analysis. A total of 28,754 flux measurements were obtained (for details see <https://doi.org/10.1594/IEDA/100672>), each with an estimated uncertainty of $< 26\%$ (after Galle et al., 2010). This uncertainty mostly comes from uncertainty in wind speed data, since radiative transfer effects are likely less important due to close proximity to an ash-free plume. Available SO_2 flux data were averaged to obtain mean values for each valid Multi-GAS temporal window. The cumulative error in derived CO_2 fluxes is estimated at 40% from propagation of Multi-GAS and NOVAC uncertainties.

2.3. Space-Based Thermal Data

Thermal data acquired by MODIS sensors were analyzed using MIROVA, an automated, near-real time volcanic hot spot detection system, developed at the University of Turin (Coppola et al., 2016b; www.mirovaweb.it). The MIROVA system uses the MIR radiance measured by the two MODIS sensors (carried on Terra and Aqua NASA's satellites, respectively) that scan the entire earth surface approximately four times per day (2 nighttime and 2 daytime) with a nominal ground resolution of 1 km. These features, together with the presence of a low-gain middle infrared (MIR) channel (MODIS band 21), make MODIS particularly suitable for near-real time monitoring of worldwide volcanic activity (Coppola et al., 2013, 2016b; Rothery et al., 2005; Wright et al., 2002, 2004, 2008).

The hot spot detection algorithm consists of contextual spectral and spatial principles specifically designed to efficiently detect small-scale to large-scale thermal anomalies (from < 1 MW to > 40 GW) while maintaining false detections low ($< 1\%$ according to Coppola et al., 2016b). This procedure allows to track a large variety of volcanic activity, including lava flows (Coppola et al., 2017a, 2017b) and domes (Coppola et al., 2015; Werner et al., 2017), as well as strombolian activity (Coppola et al., 2014). Nonetheless, MIROVA has shown its efficiency in detecting previously unknown effusive activity at remote volcanoes (i.e., Nevados del Chillan; Coppola et al., 2016c), in tracking the development of intense fumarolic activity at Santa Ana volcano (Laiolo et al., 2017) and in detecting the recent rebirth of Nyamulagira lava lake (Coppola et al., 2016a).

The Wooster et al. (2003) formulation is used to retrieve the volcanic radiant power (VRP; W) from MODIS data, starting from hot spot pixels detected by MIROVA:

$$\text{VRP} = 1.89 \times 10^7 \times (L_{\text{MIR}} - L_{\text{MIRbk}}) \quad (1)$$

where L_{MIR} and L_{MIRbk} are the MIR radiances ($W \text{ m}^{-2} \text{ sr}^{-1} \mu\text{m}^{-1}$) characterizing the single hot spot pixel and the background. The coefficient 1.89×10^7 ($\text{m}^2 \text{ sr} \mu\text{m}$) results from best fit regression analysis between above background MIR radiance and radiant power (Wooster et al., 2003) and allows estimations of VRP ($\pm 30\%$) of hot surfaces having temperatures ranging from 600 to 1,500 K.

Visual inspection of acquired images is used to discard false alerts, isolated fires, thermal data contaminated by clouds, or images affected by poor viewing geometry conditions. Between 2015 and 2017, MIROVA

identified 282 hotspots over Masaya volcano. Of these, 8 hotspots were due to false detections, and 31 were associated with wild fires. All of these nonvolcanic sources were easily identified because they occurred at more than 5 km from the volcano summit. Of the remaining 243 thermal anomalies associated with volcanic activity, 88 images were discarded because of the presence of clouds and/or because the high satellite zenith angle (i.e., $>45^\circ$) impeded a clear view of the Masaya summit craters. The supervised VRP measurements collected during the analyzed period are listed in the supporting information Table S1.

3. Results

The MIROVA thermal record (March 2014 to March 2017; see supporting information Table S1), illustrated in Figure 2a, confirms the Masaya lava lake formation time as established by visual observations. No thermal anomaly is detected above the Masaya summit between January 2014 and December 2015 (Figure 2a). This suggests that no magma is ponding in the Santiago crater in this temporal interval, and that the thermal anomalies associated with the degassing vent(s) are below the MIROVA detection limit. The first hot spot (~ 0.9 MW) is detected on 11 December 2015, the same day of the first direct lava lake observations in the field (Global Volcanism Program, 2016). Since then, the thermal anomalies become increasingly frequent, from 1 alert per week in December 2015 up to ~ 2 alerts per day in late March 2016. At the same time, the volcanic radiant power (VRP) increases regularly, reaching >10 MW on 21 January 2016 and >100 MW on 3 April 2016. After peaking at 126 MW on 9 May 2016, the VRP fluctuates around a mean value of 60.8 MW ($1\sigma = 25.5$ MW) until March 2017 (the end of our observation interval; see supporting information Table S1).

The temporal record of CO_2/SO_2 ratios in the Masaya volcanic plume, March 2014 to March 2017, is illustrated in Figure 2b. The several data-gaps are due to recurrent damage to electronics/mechanical parts of the Multi-GAS, caused by the corrosive action of the acidic volcanic plume. Our time series is therefore divided into five subintervals (which we refer to as phases $P1$ – $P5$), during which the Multi-GAS was continually operating (Table 1).

The mean CO_2/SO_2 ratio is similar for phases $P1$ (6.3 ± 3.1), $P2$ (4.9 ± 2.0), $P4$ (5.4 ± 2.1), and $P5$ (5.5 ± 1.9) (Figure 2b). In contrast, interval $P3$, which encompasses formation of the lava lake in early December 2015, is characterized by higher mean CO_2/SO_2 ratio (12.2 ± 6.3), and peak values >20 (and up to 41) (Figure 2b and Table 1). To test if this factor >2 difference in the CO_2/SO_2 ratio between phases $P3$ and $P1$ – $P2$ – $P4$ – $P5$ is real, and not simply due to different total volcanic gas concentration in the plumes being measured, we investigate the relationship between CO_2/SO_2 ratios and peak SO_2 concentrations in Figure 2c. The peak SO_2 concentration is the maximum SO_2 value recorded within each 30 min-long Multi-GAS acquisition window and is commonly used (e.g., Shinohara et al., 2008) as a proxy for the measured plume being rich in volcanic gases, and less air diluted. As first noted at Etna by Shinohara et al. (2008), a Multi-GAS based CO_2/SO_2 ratio population is often inversely correlated to peak SO_2 concentrations in diluted-plume conditions (low peak SO_2). In our Masaya case, the gas population shows more dispersed CO_2/SO_2 ratios at low (<15 ppm) peak SO_2 concentrations (Figure 2c), but the $P3$ gases still stand out for their unusually C-rich compositions (relative to $P1$ – $P2$ – $P4$ – $P5$). In each of the five subintervals above, the CO_2/SO_2 ratio then levels out at relatively constant (and SO_2 -independent) values in dense plume conditions (>15 ppm peak SO_2 concentrations). Filtering our data set using a SO_2 threshold of 15 ppm, the filtered time series of Figure 2d is obtained. The figure confirms the CO_2/SO_2 ratio difference between phases $P3$ (10.3 ± 2.3), and $P1$ – $P2$ – $P4$ – $P5$ (means from 3.9 ± 1.1 to 5.0 ± 1.5) at statistically significant level (e.g., well above 1 standard deviation, and beyond analytical uncertainty in individual CO_2/SO_2 ratios, $\pm 15\%$). In summary, we conclude that the compositional contrast between $P3$ and $P1$ – $P2$ – $P4$ – $P5$ gas is significant at any gas concentration level reported here (both at $<$ and >15 ppm SO_2).

The anomalous CO_2/SO_2 ratio variations during period $P3$ are detailed in Figure 2e. The figure highlights a phase of anomalous CO_2/SO_2 ratio increase in mid-November 2015, followed by a drop on 26–27 November 2015, preceding the first reports of incandescence inside the Santiago crater on December 11.

The volcanic gas plume $\text{H}_2\text{O}/\text{CO}_2$ ratio also varies markedly (Figure 2f). The ratio progressively decreases in time, from $P1$ (17.3 ± 10.3), $P2$ (5.7 ± 5.1), $P3$ (3.7 ± 1.6), and $P4$ (2.3 ± 1.3), and then increased again in subinterval $P5$ (12.8 ± 10.1) (Figure 2f). In phases $P3$ and $P4$, thus, the plume exhibits more uniform, H_2O -poorer composition, relative to other temporal intervals.

Table 1
Gas Composition and Fluxes at Masaya Volcano, 2014–2017

Subinterval name	CO ₂ /SO ₂		H ₂ O/CO ₂		Mean SO ₂ flux		Mean CO ₂ flux		Mean H ₂ O flux		Total volatile flux		Magma degassing rate		Magma degassing volume		Excess ^a magma degassing volume		Excess ^b magma degassing volume		
	(M)	1σ	(M)	1σ	(kg s ⁻¹)	1σ	(kg s ⁻¹)	1σ	(kg s ⁻¹)	1σ	(kg s ⁻¹)	(kg s ⁻¹)	(m ³ s ⁻¹)	(m ³ s ⁻¹)	(Mm ³)	(Mm ³)	(Mm ³)	(Mm ³)	(m ³ s ⁻¹)	(Mm ³)	
P1	6.3	3.1	17.3	10.3	8.6	2.4	37.3	21.1	3.3 ± 0.9	3.3 ± 0.9	3.3 ± 0.9	95	3.0 ± 0.6	2.4 ± 1.3	2.4 ± 1.3	2.4 ± 1.3	2.4 ± 1.3	2.4 ± 1.3	2.4 ± 1.3	2.4 ± 1.3	
P2	4.9	2.0	5.7	5.1	7.8	1.6	26.2	11.8	61	61	95	214	3.6 ± 1.2	1.7 ± 0.8	1.7 ± 0.8	1.7 ± 0.8	1.7 ± 0.8	1.7 ± 0.8	1.7 ± 0.8	1.7 ± 0.8	
P3	12.2	6.3	3.7	1.6	9.5	3.2	81.3	40.6	123	123	214	214	4.4 ± 2.0	5.2 ± 2.6	5.2 ± 2.6	5.2 ± 2.6	5.2 ± 2.6	5.2 ± 2.6	5.2 ± 2.6	5.2 ± 2.6	
LFP	n.d.	n.d.	n.d.	n.d.	11.4	5.2							3.1 ± 1.0	8.2 ^c	8.2 ^c	8.2 ^c	8.2 ^c	8.2 ^c	8.2 ^c	8.2 ^c	8.2 ^c
P4	5.4	2.1	2.3	1.3	8.0	2.6	32.3	18.2	30	30	71	71	3.0 ± 1.3	2.1 ± 1.1	2.1 ± 1.1	2.1 ± 1.1	2.1 ± 1.1	2.1 ± 1.1	2.1 ± 1.1	2.1 ± 1.1	
P5	5.5	1.9	12.8	10.1	7.9	3.5	34.1	22.4	22.4	22.4	22.4	22.4	3.0 ± 1.3	2.2 ± 1.4	2.2 ± 1.4	2.2 ± 1.4	2.2 ± 1.4	2.2 ± 1.4	2.2 ± 1.4	2.2 ± 1.4	

Note. Results are presented for six distinct subintervals (P1–P5 and LFP, see text). Multi-GAS derived (molar) gas ratios (CO₂/SO₂ and H₂O/CO₂) are only available for subintervals P1–P5. They are expressed as mean values (± 1 standard deviation, σ) calculated by averaging all results obtained in each of the five distinct temporal windows (raw Multi-GAS data used to calculate the means are available in the EarthChem Library at <https://doi.org/10.1594/IEDA/100651>). The SO₂ flux (in kg s⁻¹) is the mean ± standard deviation obtained by averaging all valid DOAS scans of the plume in the same temporal subintervals (available at <https://doi.org/10.1594/IEDA/100672>). CO₂ and H₂O fluxes are obtained from combination of gas compositional and SO₂ flux. The total volatile flux is the sum of the three fluxes. The magma degassing rates and volume are calculated from either SO₂ or CO₂ fluxes, using a magma density of 2,600 kg m⁻³ and total (predegassing) S and CO₂ contents in magma of respectively 500 and 6,000 mg kg⁻¹. Total degassing is assumed (e.g., S and CO₂ contents in matrix glasses from erupted volcanics are neglected). ^aThe excess magma degassing volume is calculated from the magma degassing rate difference between P3 (3.6 m³ s⁻¹) and P1–P2–P4–P5 average (3.1 m³ s⁻¹). ^bThe excess magma degassing volume is calculated from the magma degassing rate difference between P3 (5.2 m³ s⁻¹) and P1–P2–P4–P5 average (2.1 m³ s⁻¹). ^cCalculated from extrapolation of the magma degassing rate over the entire duration of subinterval P3 (26 days). ^dCalculated from extrapolation of the magma degassing rate over the entire duration of subinterval PLF (64 days).

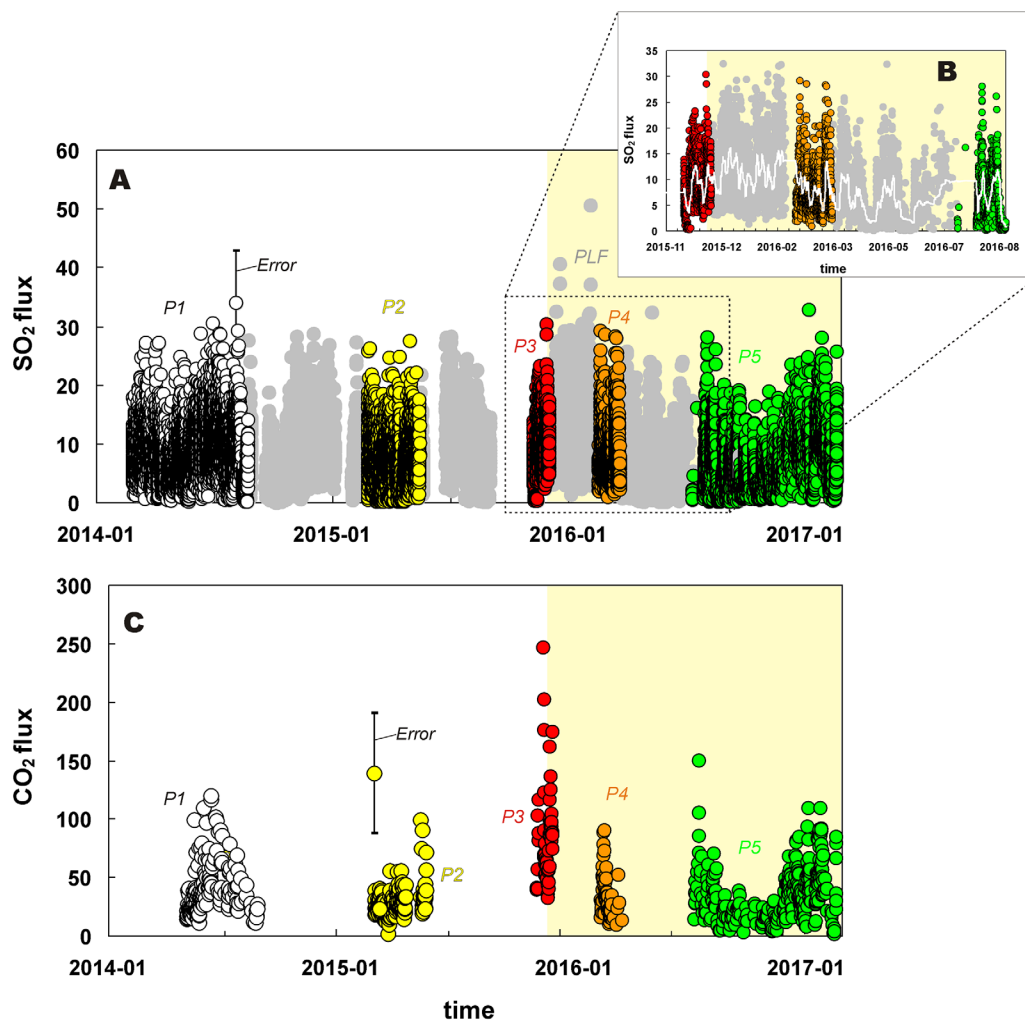


Figure 3. (a) Time series of the volcanic SO₂ flux (kg s⁻¹), January 2014 to February 2015, based on measurements with a permanent scanning-DOAS of the NOVAC network. Data obtained during the five Multi-GAS acquisition subintervals are colored as in Figure 2, grey symbols identify DOAS data with no contemporaneous compositional (Multi-GAS) record, including the phase of lake formation (PLF). (b) Zoom of Figure 3a for the period before and during lava lake formation. The white line is a 3 month moving average. The SO₂ flux peaks in the PLF phase. (c) Time series of the volcanic CO₂ flux (kg s⁻¹), calculated combining sets of coacquired CO₂/SO₂ ratio values (of Figure 2b) and SO₂ fluxes (the DOAS records closest in time to each 30 min Multi-GAS temporal interval are averaged and used for scaling). The CO₂ flux peaks in the P3 subinterval, right before appearance of the lava lake. Error bars for some representative measurement points are shown.

The NOVAC-based SO₂ flux time series (Figure 3a) is more continuous than the Multi-GAS time series. Each of the five phases above exhibits a wide SO₂ flux range, with no obvious temporal trend, the mean SO₂ fluxes (± 1 standard deviation) being: P1 (8.6 ± 2.4 kg/s), P2 (7.8 ± 1.6 kg/s), P3 (9.5 ± 3.2 kg/s), P4 (8.0 ± 2.6 kg/s), and P5 (7.9 ± 3.5 kg/s). The mean SO₂ flux in interval P3 is thus close, or only slightly (17%) higher than, the 8.0 kg/s average for P1–P2–P4–P5. The highest peak SO₂ fluxes (up to 50.7 kg/s) are recorded in the temporal interval between P3 and P4, e.g., between 11 December 2015 and 15 February 2016 (Figure 3b), when the lava lake was first visually observed and was reported to be more vigorously degassing (Global Volcanism Program, 2016). The mean SO₂ flux in this *phase of lake formation* (PLF) is 11.4 ± 5.2 kg/s, or 40% higher than the P1–P2–P4–P5 average (8.0 kg/s). We yet caution that this SO₂ flux increase, while significant (Figure 3b), is still within uncertainty (45%). Our SO₂ flux results (Figure 3a), including those in the PLF, are within the range of those obtained by de Moor et al. (2017). These authors conducted periodic surveys at a number of Central American volcanoes including Masaya (12 measurements between November

2015 and July 2016), where SO₂ fluxes of 10.1–58.1 kg/s were obtained using the traverse technique (e.g., traversing underneath the plume with a vertically pointed DOAS).

The volcanic CO₂ flux time series (Figure 3c) is calculated by multiplying each CO₂/SO₂ ratio value (of Figure 2b) by the time-averaged SO₂ flux during the same temporal interval. The CO₂ flux peaks during subinterval P3 (mean, 81.3 ± 40.6 kg/s; maximum, 247 kg/s on 25 November 2015). Both the mean (26.2–37.3 kg/s, Table 1) and maximum (149 kg/s) CO₂ flux are systematically lower during subintervals P1–P2–P4–P5. For comparison, the CO₂ flux results reported in de Moor et al. (2017) range from 50 to 161 kg/s (10 measurements between November 2015 and July 2016).

4. Discussion

Visual observations and satellite data concur to indicate that a stable, vigorously degassing lava lake resumed at Masaya on 11 December 2015 (Figures 1 and 2a), after ~3 years of passive degassing but no visible incandescence (Global Volcanism Program, 2016). The lava lake has been, since its formation, a sizeable heat source. By using the volcanic radiant power (VRP) results illustrated in Figure 2a, we estimate a cumulative thermal radiance from the Masaya lava lake, between 11 December 2015 and 31 December 2016, of $\sim 1.53 \pm 0.46 \cdot 10^{15}$ J, and a mean radiant flux of 46.5 ± 3.9 MW. This radiant power is similar to the long-term thermal output produced by the Erta Ale lava lake (20–100 MW; Barnie et al., 2016 and references therein), which yet contributes an order of magnitude less SO₂ (~1.3 kg/s; Oppenheimer et al., 2004). The Masaya radiant flux is only ~5–10% the radiant power recently recorded above the Nyiragongo lava lake (~1,000 MW; Coppola et al., 2016a; Spampinato et al., 2013).

The presence of an operating ground-based gas observational network, combined with satellite thermal sensing, allows us to track resumption of lava lake activity with relatively high temporal resolution, and to derive novel information on the driving magmatic processes.

4.1. A CO₂-Rich Gas

Since onset of the 1993 to present degassing unrest, and prior to our study, the H₂O–CO₂–SO₂ signature of the Masaya volcanic gas plume has been determined in six occasions during field surveys in 1998, 1999, 2000, 2001, 2006, and 2009 (see Martin et al., 2010 for a review). These previous studies indicated plume CO₂/SO₂ ratios of 1.5–3.5 (mean: 2.5 ± 0.7) and a hydrous gas signature (H₂O/CO₂ ratios of 27.9 ± 11.2) (Figure 4a).

Our systematic gas observations demonstrate a systematically more CO₂-rich gas vented by Masaya in 2014–2017 (Figure 4a). The time-averaged (all data, 2014–2017 period) CO₂/SO₂ ratio is 6.2 ± 3.5 (range 2.2–41), well beyond the 1998–2009 range. Our derived H₂O/CO₂ ratios are also lower (2014–2017 average: 10.3 ± 8.8). An especially CO₂-rich composition (Figures 2 and 4a) is observed in mid to late-November 2015 (our subinterval P3), a few weeks prior to “rebirth” of the Masaya lava lake in December 2015. In the same subinterval P3, the CO₂ flux (Figure 3c) is 2–3 times the average 2014–2017 levels (26.2–37.3 kg/s), and 7.5 times the Martin et al. (2010) estimate of ~10.7 kg/s (in March 2009). After P3, gas parameters (composition and fluxes) are back to P1–P2 levels. In summary, our results point to a perturbed degassing regime at Masaya in 2014–2017 and suggest unusually elevated CO₂ release prior to appearance of the lava lake in late 2015.

4.2. Measured Versus Modeled Gas Compositions

The time-evolving volcanic gas composition in 2014–2017 and especially the elevated CO₂ degassing phase P3 are quantitatively interpreted from results of model runs performed with a volatile saturation code (Figure 4). As in previous work (Aiuppa et al., 2007, 2010, 2016; de Moor et al., 2016), the model of Moretti et al. (2003) and Moretti and Papale (2004) is used to simulate the pressure-dependent compositional evolution (in the C–O–H–S system) of the Masaya magmatic gas phase formed upon magma decompression in the 400–0.1 MPa interval (Figure 4b).

The model runs are initialized at conditions representative of the Masaya magmatic system (Table 2). Temperature is set constant throughout the runs at 1,116°C (from de Moor et al., 2013, calculated from the olivine-liquid geothermometer of Putirka (2008)). Oxygen fugacity of Masaya melt is fixed at 1.7 Log units above the QFM ($\Delta\text{QFM} = +1.7$, whereby QFM is the quartz-fayalite-magnetite buffer of Frost (1991)), based

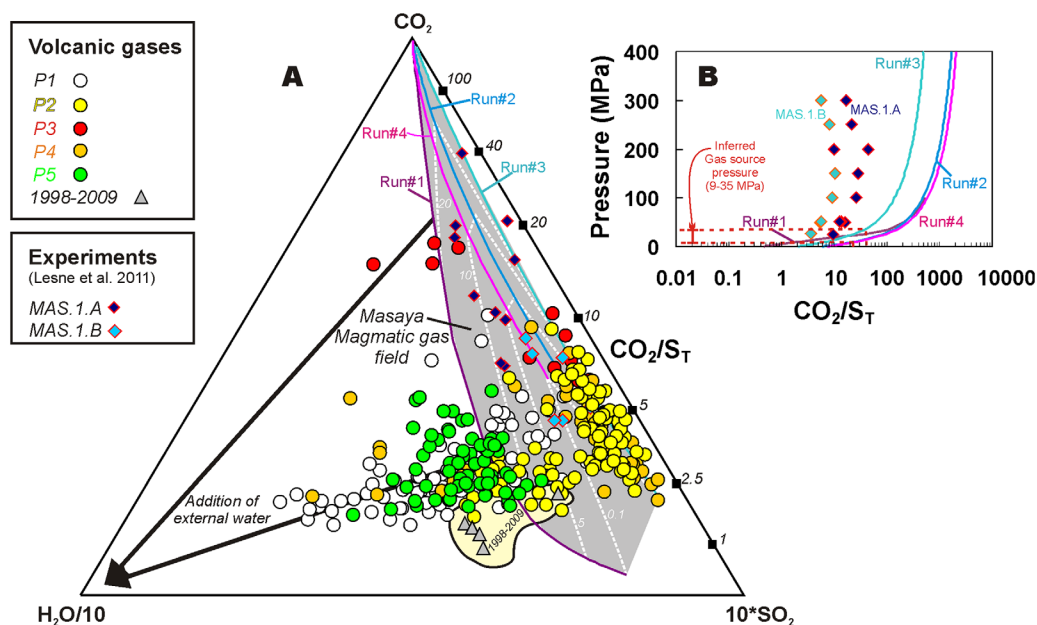


Figure 4. (a) Triangular plot comparing the measured compositions of Masaya volcanic gases (circles; symbols as in Figure 2) with model gas compositions calculated in the four model runs with the saturation model of Moretti et al. (2003). Runs #1 to #4 differ in the model initialization parameters used (see Table 2 for details) but all describe a pressure-dependent magmatic gas evolution, from CO₂ rich (high pressure) to SO₂ rich (low pressure). Isobars are indicated by the white dashed lines (numbers stand for pressure, in MPa). The model lines confine the Masaya magmatic gas field (grey filled area). The calculated experimental fluid compositions (MAS.1.A and MAS.1.B) of Lesne et al. (2011) consistently fall within this magmatic field. However, different initial conditions prevent a quantitative comparison between model results and experimental runs (see text for details). Volcanic gas samples obtained in 2014–2017 (this study) are systematically richer in CO₂ relative to 1998–2009 gas data (triangles, see Martin et al., 2010 for data source). P1 and P5 gases mostly fall out of the Masaya magmatic gas field, suggesting addition of nonmagmatic (meteoric or atmospheric) H₂O. P3 gases are the richest in CO₂, implying separation pressures of >10 MPa. (b) Pressure dependence of the (molar) CO₂/S_T ratio in the four model runs (S_T stands for total S, and corresponds to SO₂ + H₂S at the conditions explored here). Runs#1, #2, and #4 output overall consistent trends, while the S-rich run#3 yields systematically lower CO₂/S_T ratio compositions. A gas source pressure of 9–35 MPa is inferred by combining the measured P3 gas compositions with the model trends. The experimental fluids of Lesne et al. (2011) diverge from the model trends at high pressure and are shifted to lower CO₂/S_T ratios. We ascribe this to higher H₂O contents and formation of solid/liquid sulphides in the experiments of Lesne et al. (2011).

on measured iron speciation (de Moor et al., 2013). Melt composition and total volatile contents (Table 2) are inferred from compositions of Masaya melt inclusions (MIs; Atlas & Dixon, 2006; de Moor et al., 2013; Sadofsky et al., 2008; Wehrmann et al., 2011; Zurek, 2016) and glasses from laboratory degassing experiments performed at Masaya-like conditions (Lesne et al., 2011).

Melt inclusion results suggest that Masaya volcano is fed by relatively water-poor (1.5–1.6 wt %) magma, similar to other primitive magmas in Central Nicaragua (e.g., Granada and Nejapa volcanoes; Wehrmann et al., 2011). Available melt inclusion data for Masaya show therefore no evidence of the water-rich (H₂O = 3.0–6.1 wt %) magma component seen at other Nicaraguan volcanoes, including Cerro Negro, Telica, San Cristóbal, and Cosigüina (Longpré et al., 2014; Portnyagin et al., 2014; Robidoux et al., 2017a, 2017b; Roggensack et al., 1997). Note that although the degassing experiments of Lesne et al. (2011) were initially prepared and run at 1.5–1.7 wt % H₂O, final total H₂O contents in experimental charges (fluid + glass) were >2.6 wt % because of water production due to hydrogen exchange and reduction of ferric iron (Lesne et al., 2011; Table 2). The experimental results of Lesne et al. (2011) are unique for Masaya, but their higher (than MIs) H₂O contents are likely to have determined vapor-melt partitioning unrepresentative of natural conditions (see below). The Lesne's et al. (2011) experiments will be thus considered in the following for comparative purposes only, but not as stringent constraints for our interpretation.

Melt inclusion information also converges to indicate a preeruptive S content of ~500 mg kg⁻¹ (Table 2). This implies that the MAS.1.A experiment of Lesne et al. (2011) (our run#2) is likely the closest to natural conditions (apart from the aforesaid issues on the total water content), while the MAS.1.B experiment of

Table 2
Initialization Parameters of Model Runs

Run ID	Run conditions	T (°C)	fO ₂ (ΔQFM)	log fO ₂	H ₂ O (wt %)	CO ₂ (mg kg ⁻¹)	S (mg kg ⁻¹)	SiO ₂ (wt %)	TiO ₂ (wt %)	Al ₂ O ₃ (wt %)	FeO ^a (wt %)	MnO (wt %)	MgO (wt %)	CaO (wt %)	Na ₂ O (wt %)	K ₂ O (wt %)	P ₂ O ₅ (wt %)	Source (major and volatile element composition)
Run#1	Closed-system from saturation to 0.1 MPa	1,116	1.7	-7.63	1.59	369	411	53.23	1.22	15.80	11.97	0.25	3.95	8.78	3.02	1.48	0.31	Wehrmann et al. (2011)
Run#2	Closed-system from saturation to 0.1 MPa	1,116 ^c	1.7	-7.63	1.54 (2.74) ^a	7,000	595	49.39	1.24	19.16	13.26	0.25	3.58	8.53	3.31	1.51	0.31	MAS.1.A; Lesne et al. (2011)
Run#3	Closed-system from saturation to 0.1 MPa	1,116 ^c	1.7	-7.63	1.66 (2.86) ^a	7,000	1,700	49.42	1.18	18.76	12.44	0.25	3.17	8.7	3.3	1.29	0.31	MAS.1.B; Lesne et al. (2011)
Run#4	Closed-system from saturation to 0.1 MPa	1,116 ^c	1.7	-7.63	1.56	6,000 ^b	400	52.4	1.2	15.5	11.7	0.2	3.9	8.7	3.0	1.5	0.31	Sadofsky et al. (2008) Except b, from Atlas and Dixon (2006)

Note. Runs are isothermal at 1,116°C (from the de Moor et al., 2013, calculated from the olivine-liquid geothermometer of Putirka (2008)) and at oxygen fugacity of 1.7 Log units above the QFM (ΔQFM = +1.7, whereby QFM is the quartz-fayalite-magnetite buffer of Frost (1991)). Volatile contents and major elements are from melt inclusion studies on Masaya volcanics or results of degassing experiments on Masaya-like melts (Lesne et al., 2011). ^aThe Masaya experiments in Lesne et al. (2011) were actually carried out at a total water content increased by 1.2 wt % relative to initial run charges (1.54 wt % and 1.66, respectively), due to water production via reaction $Fe_2O_{3(melt)} + H_2O_{(vap)} \rightleftharpoons 2FeO_{(melt)} + H_2O_{(vap)}$. ^bAtlas and Dixon (2006).

Lesne et al. (2011) (our run#3) should only be viewed as a hypothetical S-rich example. As commonly observed at arc volcanoes (Wallace, 2005; Wallace et al., 2015), the preeruptive melt CO₂ content is the least well constrained. Wehrmann et al. (2011) reported one single inclusion with a measured CO₂ content of 369 mg kg⁻¹, and this is used as the basis for our run#1 simulation. In run#4, we consider a CO₂-richer magmatic content, based on the maximum melt inclusion CO₂ content (~6,000 mg kg⁻¹) of Atlas and Dixon (2006). Lesne et al. (2011) assumed a similarly high CO₂ content (~7,000 mg kg⁻¹; adopted in our runs#2 and #3).

Model results (Figure 4) show that, at any explored condition, the magmatic gas in equilibrium with the Masaya melt is rich in CO₂ at high pressure. As pressure decreases, the gas composition becomes H₂O-dominated and richer in S in all model runs (Figure 4). The different model trends obtained in the four runs reflect the distinct initial volatile contents used, with the most hydrous gas compositions obtained in the CO₂-poor run#1 and the least hydrous in the S-rich run#3. The four model lines together identify the compositional field of *Masaya magmatic gases* (Figure 4a), which also encompass the inferred compositional range of fluids formed in the experiments of Lesne et al. (2011).

The model runs also confirm the strong pressure dependence of the CO₂/S ratio (Figure 4b), as seen in other mafic systems (Aiuppa et al., 2007, 2010, 2017; de Moor et al., 2016). The model-derived CO₂/S versus pressure trends are less steep, and shifted toward CO₂-enriched compositions, relative to the experimental trends obtained by Lesne et al. (2011). This discrepancy, particularly evident at high pressure, reflects the 80% higher total water contents in the experiments of Lesne et al. (2011) (see above), which may have acted to determine a gas phase enriched in H₂O and S (at the expense of CO₂). We additionally argue that the CO₂/S ratios in the experiments of Lesne et al. (2011), being relatively constant over a wide P-range (Figure 4b), are inconsistent with a sulfur dissolution behavior simply determined by gas-melt partitioning. Rather, they suggest that the sulfur saturation content at sulfide saturation (SCSS) was likely reached during the experiments, leading to formation of solid/liquid iron sulfides (Mavrogenes & O'Neill, 1999; Moretti & Baker, 2008). Sulfide saturation, while not reported by Lesne et al. (2011), is well consistent with the hydrous nature of their experimental melts (Fortin et al., 2015; Moune et al., 2009). H₂O-rich conditions determine a high Fe²⁺/Fe_{tot} ratio (>0.7; Lesne et al., 2011 and our modeling) even at oxidation states of NNO + 1 or more (Moretti & Baker, 2008). In contrast, no sulfide separation is predicted by our model runs (conducted at the less hydrous conditions of Masaya natural melts), justifying the disagreement between model (this study) and experimental (Lesne et al., 2011) results at high pressures (Figure 4b). Model and experimental trends converge at low pressure (Figure 4b).

Comparison between models and observations (Figure 4a) suggests that the CO₂-rich gas detected in subinterval P3, prior to emergence of the lava lake (Figure 2e), cannot originate from a shallow source, e.g., from near-surface (0.1 MPa pressure) gas-melt separation. The four most CO₂-enriched P3 gases in Figure 4a, in particular, have CO₂/SO₂ ratios of 24.1–40.8. Depending on the model run used, these correspond to model magmatic gas compositions at respectively ~9–25 and ~15–35 MPa pressure (Figure 4b). Note that even higher equilibrium pressures (~100–200 MPa; Figure 4b) would be obtained using the MAS.1.A experimental fluid line of Lesne et al. (2011). In contrast, the CO₂-poorer gases observed in subintervals P1–P2–P4–P5 mostly fall within the low-pressure (0.1–10 MPa; Figure 4a) domain of the *Masaya magmatic gas* compositional field, indicating more shallow origin. A cluster of P1–P2–P4–P5 gases, finally, plots outside the *Masaya magmatic gas* field, and is displaced toward the H₂O corner. Most of the 1998–2009 Masaya gas data are similarly more H₂O rich than the predicted (model) magmatic gas compositions. We ascribe these hydrous gas compositions to entrainment of nonmagmatic H₂O in the plume. Interestingly, these H₂O-rich compositions dominate in subintervals P1, P2, and P5 (mostly referring to the Masaya wet season), while they are typically missing during subintervals P3 and P4 (Figure 2f) (encompassing a typical Masaya dry season). We argue that sampling of recirculated meteoric water, perhaps emitted by low-temperature meteoric-H₂O-dominated hydrothermal fumaroles along the inner crater's walls, may justify the nonmagmatic H₂O-rich gas compositions in subintervals P1, P2, and P5.

4.3. A Deep Trigger?

The above model results imply that the CO₂-rich signature of P3 gas is inconsistent with a shallow magma source. To preserve equilibrium compositions corresponding to ~9–35 MPa pressure, the source magmatic gas phase must have last equilibrated with (and separated from) the melt at equivalent depths of 0.36–

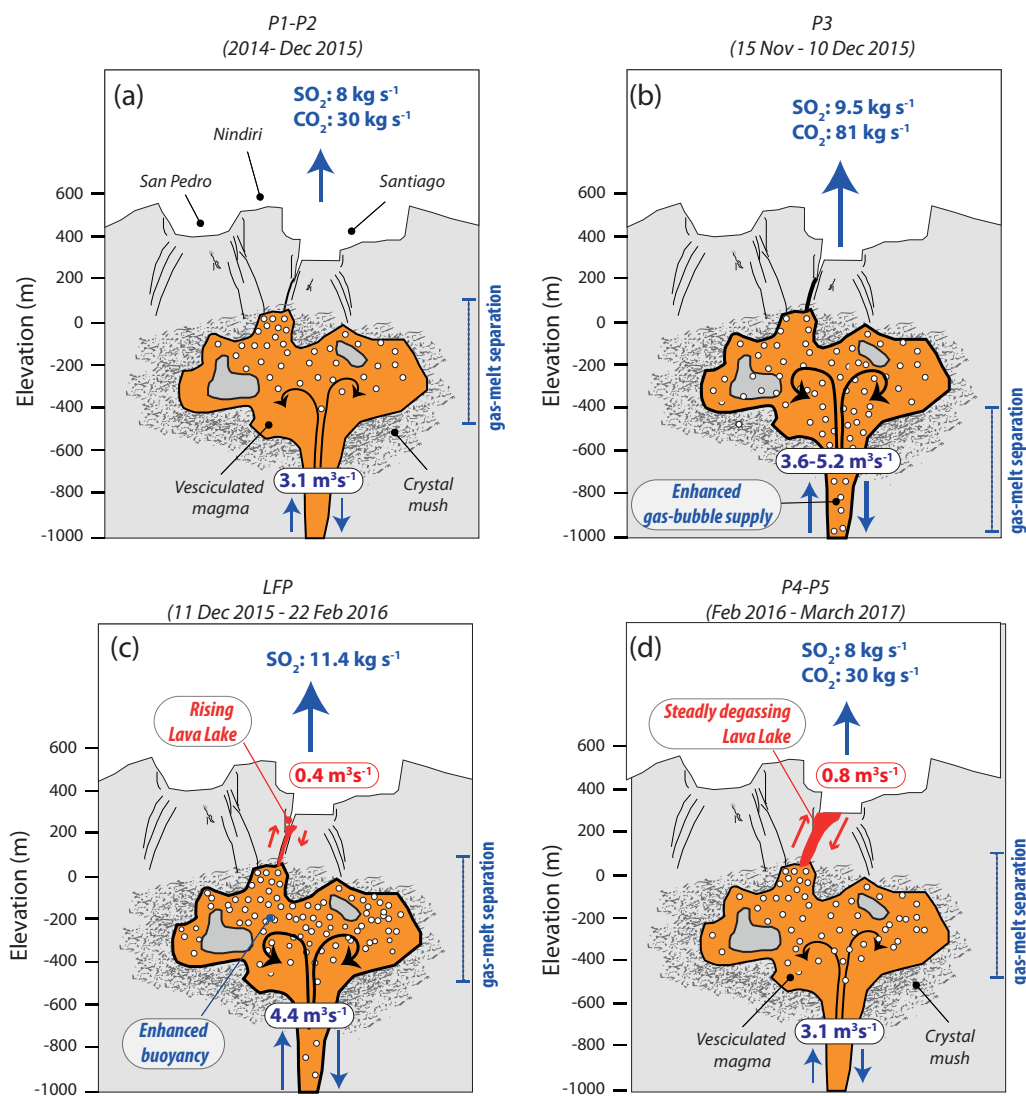


Figure 5. Cartoons showing a schematic cross section of the shallow Masaya plumbing system (modified from Rymer et al., 1998; Williams-Jones et al., 2003). (a) During subintervals *P1–P2*, SO_2 and CO_2 emissions are stable, implying magma circulation and degassing at $\sim 3.1 \text{ m}^3 \text{ s}^{-1}$. (b) The CO_2 flux peaks in phase *P3*, suggesting enhanced gas bubble supply from deep volatile-rich magma. The magma degassing rate increases ($3.6\text{--}5.2 \text{ m}^3 \text{ s}^{-1}$) and gas-melt separation level is deeper in the plumbing system ($0.36\text{--}1.4 \text{ km}$ depth). (c) Enhanced vesicularity (and thus buoyancy) of shallow resident magma, plus further magma ascent of deep-rising magma, lead to magma level rise and formation of the lake on 11 December 2015 (subinterval *LFP*). The SO_2 flux peaks at 11.4 kg s^{-1} and the lake irradiates thermal energy consisted with surface overturning of $\sim 0.4 \text{ m}^3 \text{ s}^{-1}$ of magma. (d) During subintervals *P4–P5*, the lake is now formed and steadily degassing. The surface magma circulation ($\sim 0.8 \text{ m}^3 \text{ s}^{-1}$) represents 20–30% of the magma degassing rate (returning to the pre-eruptive level of $\sim 3.1 \text{ m}^3 \text{ s}^{-1}$). The lake will likely persists until the magma supply (degassing) rate will not drop down to $\ll 3.1 \text{ m}^3 \text{ s}^{-1}$.

1.4 km (calculated using a magma density of $2,600 \text{ kg m}^{-3}$ for Masaya; Stix, 2007). This depth interval corresponds to the roots of the shallow magma reservoir identified by Rymer et al. (1998) and Williams-Jones et al. (2003), based on modeling of gravity data. According to these authors, a shallow magmatic body ($< \sim 1 \text{ km}$) is located directly beneath the currently active Nindiri cone (Figure 5), and the temporal changes in its degree of vesicularity (and thus density) govern the observed gravity variations at Masaya. Vesicularity of the shallow resident magma would, in turn, be modulated by temporal variations in gas bubble supply from deeper convecting magma (Stix, 2007), with a larger bubble influx resulting in periods of decreased gravity and elevated degassing at the surface (e.g., a degassing crisis; Delmelle et al., 1999; Williams-Jones et al., 2003).

Our observations here suggest an increasing supply of CO₂-rich gas bubbles to the shallow magmatic body (Rymer et al., 1998) in November 2015 (Figures 3c and 5b). We propose this (factor ~3) higher than usual gas bubble supply is sourced by degassing of faster convecting magma, at minimum equivalent depths of 0.36–1.4 km (Figure 5b). We infer below the increase in magma convection rate that is required to justify elevated degassing during P3.

The rate at which magma is convectively rising and degassing (*magma degassing rate*; Table 1) is initially calculated from the measured SO₂ flux, as in Williams-Jones et al. (2003) and Stix (2007). In these calculations, we use a 2,600 kg m⁻³ magma density (Stix, 2007) and assume complete degassing of a magma with 500 mg kg⁻¹ initial S content (Table 2). We neglect crystal content owing to the poorly porphyric (<<10%) nature of Masaya magmas (Zurek, 2016). Using these numbers, the mean SO₂ flux of 9.5 ± 3.2 kg s⁻¹ converts into a magma degassing rate for subinterval P3 of 3.6 ± 1.2 m³ s⁻¹ (Table 1). This calculation implies a ~20% increase in magma transport rate, relative to P1–P2–P4–P5 (mean 3.1 m³ s⁻¹; range 3.0–3.3, Table 1) is required to account for the elevated SO₂ degassing in P3. Integrated over the 26 days of duration, we infer that ~8 Mm³ must have completely degassed during P3 to account for surface SO₂ emissions, or ~1.2 Mm³ in excess to what would have degassed in the same time interval at the background rate of 3.1 m³ s⁻¹ (Table 1).

We also argue that, during P3, the SO₂ flux increases by only ~17% (relative to P1–P2–P4–P5), while the CO₂ flux increases by a factor 157% (Table 1). As such, the CO₂ flux would in principle be more appropriate to confine the magma degassing rate increase. However, this operation is complicated by the total CO₂ content in Masaya magmas being poorly constrained (Table 2). Assuming a total (parental melt) CO₂ content of 6,000 mg kg⁻¹, the P3 CO₂ flux would imply magma degassing rate of 5.2 ± 2.6 m³ s⁻¹, higher than the 3.6 ± 1.2 m³ s⁻¹ obtained above from SO₂. This mismatch is reconciled by assuming (i) a higher parental melt CO₂ content (8,600 mg kg⁻¹ of CO₂ are required to obtain a 3.6 m³ s⁻¹ magma degassing rate) or (ii) that there is deeply degassing magma that contributes lots of CO₂ but little SO₂ to the shallow convecting part of the plumbing system, or (iii) by considering that only a fraction (~70%) of total S (500 mg kg⁻¹) is actually degassed, the remaining fraction remaining dissolved in the melt. The latter is well consistent with the relatively deep (~9–35 MPa pressure) gas source in subinterval P3, and considering that the model melts still contain 295–462 mg kg⁻¹ S in dissolved form at 10 MPa (model runs #1, #2, and #4). Although we cannot entirely resolve between the three hypotheses above, owing to the lack of more precise knowledge on parental melt CO₂ content, we still consider our “deep degassing” hypothesis (a combination of (ii) and (iii) above) well motivated. The CO₂ flux-based magma degassing rate of 5.2 m³ s⁻¹ would imply a degassing magma volume (in 26 days) of 11.7 Mm³, and an excess magma degassing magma volume of ~7.2 Mm³ (Table 1).

In view of the above calculations, we consider likely that degassing of an unusually high (8.2–11.7 Mm³) magma volume, circulating at >~9–35 MPa pressure (0.36–1.4 km depth) at an average rate of 3.6–5.2 m³ s⁻¹, sustained elevated CO₂-rich gas supply during the 26 days of subinterval P3. Interestingly, our results are consistent with a general inflation of the Masaya edifice since late 2015, interpreted as due to volume change/pressure increase at ~2.3–3.8 km beneath the surface (Stephens et al., 2017; C. Wauthier, 2017, personal communication).

4.4. Formation of the Lava Lake

An elevated gas bubble supply from depth may impact stability of the shallow magma reservoir that feeds the lava lake in many different ways. According to Stix (2007), the long-lived (1993 to present) degassing unrest at Masaya, occurring with essentially no eruption of magma, can be explained by either one of the two models below (or from a combination of the two). In the *conduit convection model* (Kazahaya et al., 1994; Stevenson & Blake, 1998), persistent open-vent activity is thought to be driven by density contrast between continuously ascending (and degassing) buoyant gas-rich magma, and degassed (denser) resident magma, being recycled back in the conduit. In the *foam accumulation model* (Jaupart & Vergnolle, 1989), instead, open-vent activity is controlled by development of a foam layer at the reservoir-conduit discontinuity, in which quiescent leakage from the foam feeds continuous passive gas emissions, while catastrophic collapse of the foam (by reaching a critical thickness) generates explosive magmatic eruptions (not recently recorded at Masaya). In both models, the gas bubble supply is a critical factor. In the *conduit convection model*, gas bubbles control density of the ascending magma, with an increase in bubble supply leading to

greater buoyancy and faster convection. In the *foam accumulation model*, a larger influx of gas bubbles leads to thickening of the foam layer, increased gas transport from the foam to the conduit (and, hence, enhanced surface degassing), and to increasing magma level in the conduit. A variable gas bubble supply from depth has, for instance, been evoked as the mechanism driving lava lake level fluctuations at Erta Ale volcano in Ethiopia (Vergnolle & Bouche, 2016).

In view of these considerations, it is reasonable to establish a cause-effect relationship between the elevated gas bubble supply (and surface discharge) in subinterval *P3*, and the ensuing formation of the Masaya lava lake. Although we cannot exclude the concomitant action of additional factors, including gravitational collapse of the unstable crater floor (Harris, 2009; Rymer et al., 1998), we find it unlikely that the elevated degassing pulse in mid to late-November 2015, and the appearance of the lava lake on 11 December 2015, is a mere temporal coincidence. We propose, instead, that a combination of (i) further upward migration of the bubble-rich magma and (ii) rejuvenation of shallow resident magma by deeply sourced gas bubbles, caused the more buoyant column to migrate upward, driving collapse of the crater floor and ultimately manifesting in a vigorous lava lake (Figure 5c). No gas composition information is available for the most vigorous lava lake activity period (*PLF*; Figure 3a). However, a decreasing CO_2/SO_2 ratio is observed in the last 12 days of subinterval *P3* (Figure 2e), and a carbon-poor composition (relative to *P3*) is observed in subinterval *P4* (22 February to 28 March 2016), with the lake still being present and active (Figure 1). Our gas compositional data are therefore consistent with shallowing of the magmatic source (Figure 4).

Enhanced shallow magma convection in late 2015 to early 2016 is clearly supported by the elevated SO_2 fluxes in subinterval *PLF* (Figures 3a and 3b). The SO_2 flux during *PLF* averages at 11.4 ± 5.2 kg/s (versus the 8.1 kg/s mean for subintervals *P1–P2–P4–P5*), and implies degassing of 4.4 ± 2.0 m³ of magma per second (Table 1 and Figures 5 and 6). For the *PLF* duration of 64 days, this corresponds to convective ascent, complete degassing, and recycling of ~ 24 Mm³ of magma. The excess magma volume, e.g., the mass of magma exceeding what would have degassed in 64 days at the background rate of 3.1 m³ s⁻¹, is thus ~ 7 Mm³.

In total, we thus infer that ~ 7.2 to ~ 8.2 Mm³ more magma than during background intervals (*P1–P2–P4–P5*) circulated (and degassed) underneath Masaya between November 2015 and February 2016 (Table 1). This elevated shallow magma circulation ultimately culminated in formation and growth of the lava lake (Figure 5c).

Further clues on the processes leading to formation of the lake can be obtained by comparing the above SO_2 -derived magma degassing rate (Table 1) with the volumetric magma flux inferred from MIROVA-derived thermal data (Figure 6). In fact, while the SO_2 data allows constraint on the rate at which the

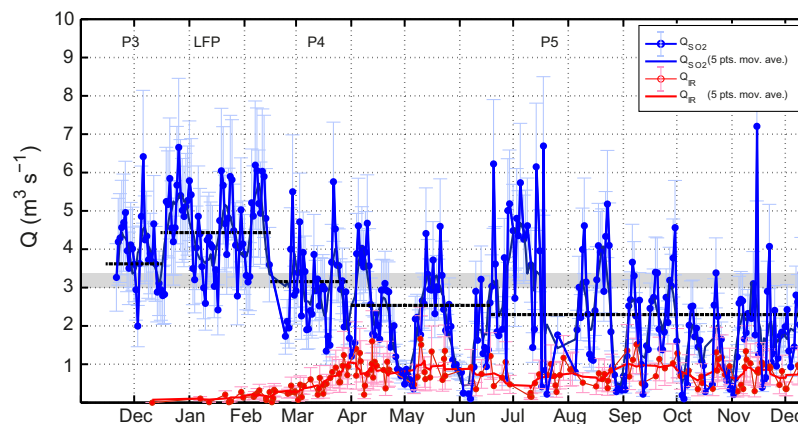


Figure 6. Time series of magma degassing rate (Q_{SO_2} , in blue) and “surficial” magma flux retrieved using thermal data (Q_{IR} in red). The two magma fluxes describe the rate of convective magma transport inside two distinct portions of the plumbing system: (i) the degassing cell located above the exsolution level of SO_2 (Q_{SO_2}) and (ii) the lava lake system at the surface. Only 1–10% of the degassing magma reaches the free surface of the lake during phases *LFP* and *P4*. The efficiency of magma transport increases up to 20–30% during *P5*, characterized by a stable magma level. The long-term mean magma degassing rate typical of Masaya is represented by the grey horizontal bar.

magma is convectively rising and degassing within the shallow plumbing system (Q_{SO_2}), the thermal data can be used to infer the rate at which the magma reaches the uppermost levels of the magma column (i.e., the lava lake), where it radiates and cools before being cycled back (Q_{IR}).

Following Coppola et al. (2013) this magma flux can be calculated from

$$Q_{IR} = \frac{VRP}{6.45 \times 10^{25} \times (X_{SiO_2})^{-10.4}} \quad (2)$$

where X_{SiO_2} is the silica content of the erupted lavas (51.5 wt % for Masaya; Walker et al., 1993). This approach and other similar thermal proxies (see Harris & Baloga, 2009) are commonly applied during effusive eruptions in order to estimate the “TimeAveraged Lava Discharge Rate” (*TADR*) feeding an active lava flow. The typical error associated with satellite-based estimates of magma flux is $\pm 50\%$, a value comparable with field-based estimates (Coppola et al., 2013; Harris et al., 2007). This uncertainty mostly comes from the implicit assumption of two end-member thermorheological models (defined as hot and cold models by Harris et al. (2007)) that may characterize the spreading and cooling processes of active lava flows. The two models thus provide an upper and lower value of magma flux for any VRP measurement, being representative of large areas/poorly insulated conditions (the hot model – higher radiant density) and small areas/highly insulated conditions (the cold model – lower radiant density). The real volumetric flux may thus vary within these two boundary estimates depending on the local conditions of area and temperature.

In the case of a convecting lava lake, where no magma is discharged from the magmatic system, the thermal proxy (equation (2)) can be used to evaluate what would be the equivalent magma discharge rate in the absence of magma recycling (Coppola et al., 2012, 2013). This corresponds to the volumetric magma flux that would need to be supplied to a lava flow in order to radiate an equivalent amount of thermal energy into the atmosphere. In other words, Q_{IR} provides the rate at which magma is supplied to the surface before being “discharged” (effusive eruptions) or cycled back into the feeding system (lava lakes/open vent volcanoes).

In this view, we interpret the two magma fluxes (Q_{SO_2} and Q_{IR}) as sampling the rate of magma transport at different depths, being the SO_2 -derived flux relative to the magma circulation above the exsolution level of SO_2 , and the IR-derived flux relative to surficial magma circulation (i.e., few tens of meters at most; Figure 6). The two magma fluxes may be nonsynchronous due, for example, to the different ascent rate of gas and magma within the shallow plumbing system, or due to the delay it takes a degassing-induced collapses in the crater to reveal the magma. However, on a reasonable time scale of few days, the two fluxes can only be equivalent in the limit condition that all magma entering and degassing within the shallow plumbing system ultimately reaches the free air-magma interface.

During subinterval *P3*, Q_{IR} is equal to zero (Figures 5b and 6), since no lava lake is exposed at the bottom of the Santiago crater. However, the higher than normal magma degassing rate (see section 4.3) suggests ascent (and degassing) of a new batch of gas-rich magma in the magmatic system (see above, Figure 5b). We propose that such increased gas supply, and the added magma volume, lead to overpressurization of the shallow magmatic system, causing a gradual rise of the magma column and the subsequent appearance of the lava lake during subinterval *PLF* (Figure 5c). During this period, the magma degassing rate (Q_{SO_2}) is enhanced by $\sim 0.8 \text{ m}^3 \text{ s}^{-1}$, thus reaching $\sim 4.4 \text{ m}^3 \text{ s}^{-1}$ (Figure 6). At the same time, Q_{IR} gradually increases from 0 to $\sim 0.4 \text{ m}^3 \text{ s}^{-1}$ (about one tenth of the total SO_2 -derived flux), suggesting that $\leq 10\%$ of the degassing magma can finally make its way to the surface in a lava lake (Figure 6). The progressive increase in the magma level continues until March 2016, when Q_{IR} stabilizes at $\sim 0.8 \text{ m}^3 \text{ s}^{-1}$ and the *magma degassing rate* returns back to normal values (i.e., $\sim 3 \text{ m}^3 \text{ s}^{-1}$) (Figure 6). In these periods (*P4* and *P5*; Figure 5d), the proportion of degassing magma reaching the free surface of the lake increases to $\sim 20\text{--}30\%$, thus suggesting an improved, but still incomplete efficiency of the plumbing system in transporting the ascending magma up to the free surface. This condition persists to the time of writing, and will likely continue until a further decrease of the magma degassing rate (e.g., in magma feeding into the shallow plumbing system) may cause the lava lake to disappear (as previously seen at Masaya in historical time). On the contrary, the upper limit condition of magma transport efficiency ($\sim 100\%$, i.e., with all the degassing magma reaching the lava lake) would be hypothetically reached for $Q_{IR} = Q_{SO_2} \cong 3.1 \text{ m}^3 \text{ s}^{-1}$, at which the lava lake would be radiating $\sim 400 \text{ MW}$ (equation (2)). In view of the rarity of historical eruptions at Masaya, this condition is

reached very infrequently. However, a maximum efficiency of transport to the surface could result in further rise of the lava lake level or even eventual production of a lava flow.

4.5. Comparison With Other Lava Lakes

The calculations above suggest an evident unbalance between magma input (Q_{SO_2}) and output (Q_{IR}) at Masaya. We speculate this unbalance may be causing the rarity of overflow or lateral eruptions at this volcano, and perhaps at other systems (e.g., Villarrica and Erebus) that exhibit similarly stable lava lakes. We anticipate that a systematic analysis of Q_{SO_2} versus Q_{IR} relationships is required to test, and eventually corroborate, our hypothesis, including observations and modeling at those lava lakes characterized by more dynamic eruptive behavior (such as Nyiragongo (Burgi et al., 2014) and Erta Ale (Vergnolle & Bouche, 2016)).

The Q_{SO_2} versus Q_{IR} unbalance at Masaya requires a very efficient extraction of gas bubbles from the melt, perhaps due to reduced melt viscosity (in the $\sim 10^2$ Pa s order; Stix, 2007). Gas separation from melt during open-system degassing drives sinking of degassed magma back into the conduit (Shinohara, 2008), thus posing a limit to the surface emplaced magma volume (Q_{IR}).

The contrasting magma rheologies can also justify the distinct 2015 behaviours of Masaya and Villarrica lava lakes (degassed, crystal-rich basaltic andesites feeding the Villarrica lava lake have inferred viscosity in the $\sim 10^3$ Pa s range (Witter et al., 2004), or a factor 10 higher than Masaya). As reported by Aiuppa et al. (2017), a period of elevated supply of deeply sourced CO_2 -rich gas bubbles, similar in duration and magnitude to that seen at Masaya (this study), was observed in early 2015 at Villarrica. However, the elevated CO_2 degassing phase at Villarrica culminated into a violent (VEI, Volcanic Explosivity Index = 2) paroxysmal explosion, while no eruption was observed at Masaya, only the emergence of a vigorously degassing lava lake. A combination of different initial volatile contents, magma overpressures, and decompression rates, in addition to distinct magma rheologies, may have concurred to explain the contrasting volcanic behaviours. In any case, the “quiet” lava lake emergence at Masaya is clearly indicative of efficient magma degassing.

5. Conclusions

We have presented novel ground-based (volcanic gas) and space-based (thermal) observations to systematically characterize a (re)formation event of the Masaya lava lake for the first time. Our results show that appearance of the lava lake in December 2015 was anticipated in mid to late-November by a noticeable volcanic gas plume compositional change toward more CO_2 -rich compositions, and by a sizeable CO_2 flux increase. We interpret these observations as evidence for usual supply of CO_2 -rich gas bubbles, sourced by enhanced (3.6 – 5.2 m^3 s^{-1}) magma transport and degassing at $> \sim 9$ – 35 MPa pressure (0.36 – 1.4 km depth). This interpretation is consistent with a measured (late 2015 to early 2016) inflation, having an inferred deformation source at ~ 2.3 – 3.8 km depth km beneath the surface (Stephens et al., 2017; C. Wauthier, 2017, personal communication). Further upward magma migration, and/or rejuvenation of shallow resident magma by deep-rising gas bubbles, ultimately caused the lava lake to appear on 11 December 2015. Shallow-level, faster than normal (4.4 versus ~ 3 m^3 s^{-1}) magma circulation since mid-December 2015 is proved by a return to more SO_2 -rich composition, by a $\sim 40\%$ SO_2 flux increase, and by a progressive volcanic radiant power increase, peaking at 126 MW in May 2016. Modeling of the thermal anomaly irradiated by the lava lake is consistent with a lava lake supplied at ~ 0.4 – 0.8 m^3 s^{-1} rate, implying that only ~ 10 – 30% of shallow circulating (and degassing) magma (4.4 – 3.1 m^3 s^{-1}) ultimately reached the surface. We anticipate the lava lake will likely persist until magma feeding in the shallow plumbing system declines to $\ll 3$ m^3 s^{-1} .

References

- Aiuppa, A., Bertagnini, A., Métrich, N., Moretti, R., Di Muro, A., Liuzzo, M., et al. (2010). A model of degassing for Stromboli volcano. *Earth and Planetary Science Letters*, 295, 195–204.
- Aiuppa, A., Bitetto, M., Francoforte, V., Velasquez, G., Parra, C. B., Giudice, G., et al. (2017). A CO_2 -gas precursor to the March 2015 Villarrica volcano eruption. *Geochemistry, Geophysics, Geosystems*, 18, 2120–2132. <https://doi.org/10.1002/2017GC006892>
- Aiuppa, A., Federico, C., Giudice, G., & Gurrieri, S. (2005). Chemical mapping of a fumarolic field: La Fossa Crater, Vulcano Island (Aeolian Islands, Italy). *Geophysical Research Letters*, 32, L13309. <https://doi.org/10.1029/2005GL023207>
- Aiuppa, A., Lo Coco, E., Liuzzo, M., Giudice, G., Giuffrida, G., & Moretti, R. (2016). Terminal Strombolian activity at Etna's central craters during summer 2012: The most CO_2 -rich volcanic gas ever recorded at Mount Etna. *Geochemical Journal*, 50(2), 123–138.

Acknowledgments

This research received funding from the Deep Earth CARbon DEgassing (DECADE) program of the Deep Carbon Observatory (DCO), and by the European Research Council (ERC) (grant agreement 305377 of the Framework Programme 7) (Pi, Aiuppa). Field support in terms of vehicles and equipment was provided by OVSICOR-UNA and INETER. Raw (mixing ratio) and processed (molar ratio) Multi-GAS data and processed NOVAC data are downloadable from the EarthChem Library at <https://doi.org/10.1594/IEDA/100651> and <https://doi.org/10.1594/IEDA/100672>, respectively. Insightful comments by Tamsin Mather and an anonymous reviewer contributed to improving the quality of the manuscript.

- Aiuppa, A., Moretti, R., Federico, C., Giudice, G., Gurrieri, S., Liuzzo, M., et al. (2007). Forecasting Etna eruptions by real-time observation of volcanic gas composition. *Geology*, 35(12), 1115–1118.
- Aiuppa, A., Robidoux, P., Tamburello, G., Conde, V., Galle, B., Avar, G., et al. (2014). Gas measurements from the Costa Rica-Nicaragua volcanic segment suggest possible along-arc variations in volcanic gas chemistry. *Earth and Planetary Science Letters*, 407, 134–147.
- Allard, P., Aiuppa, A., Bani, P., Métrich, N., Bertagnini, A., Gauthier, P. J., et al. (2015). Prodigious emission rates and magma degassing budget of major, trace and radioactive volatile species from Ambrym basaltic volcano, Vanuatu island Arc. *Journal of Volcanology and Geothermal Research*, 304, 378–402.
- Atlas, Z. D., & Dixon, J. E. (2006). Interconnected magmatic conduit systems as recorded by melt inclusions from Masaya and Apoyo Calderas, Nicaragua. *Eos, Transactions of the American Geophysical Union*, 87(52), Fall Meet. Suppl., Abstract V13D-06.
- Barnie, T. D., Oppenheimer, C., & Pagli, C. (2016). Does the lava lake of Erta 'Ale volcano respond to regional magmatic and tectonic events? An investigation using Earth Observation data. *Geological Society Special Publication*, 420(1), 181–208.
- Bice, D. C. (1985). Quaternary volcanic stratigraphy of Managua, Nicaragua: Correlation and source assignment for multiple overlapping plinian deposits. *Geological Society of America Bulletin*, 96, 553–566.
- Buck, A. L. (1981). New equations for computing vapor pressure and enhancement factor. *Journal of Applied Meteorology*, 20(12), 1527–1532.
- Burgi, P. Y., Darrah, T. H., Tedesco, D., & Eymold, W. K. (2014). Dynamics of the Mount Nyiragongo lava lake. *Journal of Volcanology and Geothermal Research*, 119(5), 4106–4122.
- Burton, M. R., Oppenheimer, C., Horrocks, L. A., & Francis, P. W. (2000). Remote sensing of CO₂ and H₂O emission rates from Masaya volcano, Nicaragua. *Geology*, 28(10), 915–918.
- Coppola, D., Campion, R., Laiolo, M., Cuoco, E., Balagizi, C., Ripepe, M., et al. (2016a). Birth of a lava lake: Nyamulagira volcano 2011–2015. *Bulletin of Volcanology*, 78(3), 1–13.
- Coppola, D., Di Muro, A., Peltier, A., Villeneuve, N., Ferrazzini, V., Favalli, M., et al. (2017b). Shallow system rejuvenation and magma discharge trends at Piton de la Fournaise volcano (La Réunion Island). *Earth and Planetary Science Letters*, 463, 13–24.
- Coppola, D., Laiolo, M., Cigolini, C., Delle Donne, D., & Ripepe, M. (2016b). Enhanced volcanic hot-spot detection using MODIS IR data: Results from the MIROVA system. *Geological Society Special Publication*, 426(1), 181–205.
- Coppola, D., Laiolo, M., Delle Donne, D., Ripepe, M., & Cigolini, C. (2014). Hot-spot detection and characterization of Strombolian activity from MODIS infrared data. *International Journal of Remote Sensing*, 35(9), 3403–3426.
- Coppola, D., Laiolo, M., Lara, L. E., Cigolini, C., & Orozco, G. (2016c). The 2008 “silent” eruption of Nevados de Chillán (Chile) detected from space: Effusive rates and trends from the MIROVA system. *Journal of Volcanology and Geothermal Research*, 327, 322–329.
- Coppola, D., Laiolo, M., Piscopo, D., & Cigolini, C. (2013). Rheological control on the radiant density of active lava flows and domes. *Journal of Volcanology and Geothermal Research*, 249, 39–48.
- Coppola, D., Macedo, O., Ramos, D., Finizola, A., Delle Donne, D., del Carpio, J., et al. (2015). Magma extrusion during the Ubinas 2013–2014 eruptive crisis based on satellite thermal imaging (MIROVA) and ground-based monitoring. *Journal of Volcanology and Geothermal Research*, 302, 199–210.
- Coppola, D., Piscopo, D., Laiolo, M., Cigolini, C., Delle Donne, D., & Ripepe, M. (2012). Radiative heat power at Stromboli volcano during 2000–2011: Twelve years of MODIS observations. *Journal of Volcanology and Geothermal Research*, 215–216, 48–60.
- Coppola, D., Ripepe, M., Laiolo, M., & Cigolini, C. (2017a). Modelling satellite-derived magma discharge to explain caldera collapse. *Geology*, 45(6), 523–526.
- Dee, D. P., Uppala, S. M., Simmons, A. J., Berrisford, P., Poli, P., Kobayashi, S., et al. (2011). The ERA-Interim reanalysis: Configuration and performance of the data assimilation system. *Quarterly Journal of the Royal Meteorological Society*, 137(656), 553–597. <https://doi.org/10.1002/qj.828>
- Delmelle, P., Baxter, P., Beaulieu, A., Burton, M., Francis, P., Garcia-Alvarez, J., et al. (1999). Origin, effects of Masaya volcano's continued unrest probed in Nicaragua. *Eos, Transactions of the American Geophysical Union*, 80(48), 575–581.
- Delmelle, P., Stix, J., Baxter, P., Garcia-Alvarez, J., & Barquero, J. (2002). Atmospheric dispersion, environmental effects and potential health hazard associated with the low-altitude gas plume of Masaya volcano, Nicaragua. *Bulletin of Volcanology*, 64(6), 423–434.
- de Moor, J. M., Aiuppa, A., Avar, G., Wehrmann, H., Dunbar, N., Muller, C., et al. (2016). Turmoil at Turrialba Volcano (Costa Rica): Degassing and eruptive processes inferred from high-frequency gas monitoring. *Journal of Geophysical Research: Solid Earth*, 121, 5761–5775. <https://doi.org/10.1002/2016JB013150>
- de Moor, J. M., Fischer, T. P., Sharp, Z. D., King, P. L., Wilke, M., Botcharnikov, R. E., et al. (2013). Sulfur degassing at Erta Ale (Ethiopia) and Masaya (Nicaragua) volcanoes: Implications for degassing processes and oxygen fugacities of basaltic systems. *Geochemistry, Geophysics, Geosystems*, 14, 4076–4108. <https://doi.org/10.1002/ggge.20255>
- de Moor, J. M., Kern, C., Avar, G., Muller, C., Aiuppa, A., Saballos, A., et al. (2017). A new sulfur and carbon degassing inventory for the Southern Central American Volcanic Arc: The importance of accurate time-series data sets and possible tectonic processes responsible for temporal variations in arc-scale volatile emissions. *Geochemistry, Geophysics, Geosystems*, 18, 4437–4468. <https://doi.org/10.1002/2017GC007141>
- Duffell, H. J., Oppenheimer, C., Pyle, D. M., Galle, B., McGonigle, A. J. S., & Burton, M. R. (2003). Changes in gas composition prior to a minor explosive eruption at Masaya volcano, Nicaragua. *Journal of Volcanology and Geothermal Research*, 126(3–4), 327–339.
- Fortin, M.-A., Riddle, J., Desjardins-Langlais, Y., & Baker, D. R. (2015). The effect of water on the sulfur concentration at sulfide saturation (SCSS) in natural melts. *Geochimica et Cosmochimica Acta*, 160, 100–116.
- Frost, B. R. (1991). Introduction to oxygen fugacity and its petrologic importance. In D. H. Lindsley (Ed.), *Oxide minerals: Petrologic and magnetic significance* (pp. 1–9). Chantilly, VA: Mineralogical Society of America.
- Galle, B., Johansson, M., Rivera, C., Zhang, Y., Kihlman, M., Kern, C., et al. (2010). Network for Observation of Volcanic and Atmospheric Change (NOVAC)—A global network for volcanic gas monitoring: Network layout and instrument description. *Journal of Geophysical Research: Atmospheres*, 115, D05304. <https://doi.org/10.1029/2009JD011823>
- Global Volcanism Program. (2013). Masaya (344100). In E. Venzke (Ed.), *Volcanoes of the World*, v. 4.5.5. Smithsonian Institution. <https://doi.org/10.5479/si.GVP.VOTW4-2013>. Retrieved from <http://volcano.si.edu/volcano.cfm?vn=344100>
- Global Volcanism Program. (2016). Report on Masaya (Nicaragua). In E. Venzke (Ed.), *Bulletin of the global volcanism network*, 41:8. Smithsonian Institution.
- Harris, A. J. L. (2009). The pit-craters and pit-crater-filling lavas of Masaya volcano. *Bulletin of Volcanology*, 71(5), 541–558.
- Harris, A. J. L., & Baloga, S. M. (2009). Lava discharge rates from satellite-measured heat flux. *Geophysical Research Letters*, 36, L19302. <https://doi.org/10.1029/2009GL039717>
- Harris, A. J. L., Dehn, J., & Calvari, S. (2007). Lava effusion rate definition and measurement: A review. *Bulletin of Volcanology*, 70(1), 1–22.

- Horrocks, L. A. (2001). *Infrared spectroscopy of volcanic gases at Masaya, Nicaragua*. Milton Keynes, UK: Open University.
- Jaupart, C., & Vergnolle, S. (1989). The generation and collapse of a foam layer at the roof of a basaltic magma chamber. *Journal of Fluid Mechanics*, 203, 347–380.
- Kazahaya, K., Shinohara, H., & Saito, G. (1994). Excessive degassing of Izu-Oshima volcano: Magma convection in a conduit. *Bulletin of Volcanology*, 56(3), 207–216. <https://doi.org/10.1007/BF00279605>
- Kutterolf, S., Freundt, A., & Pérez, W. (2008). Pacific offshore record of Plinian arc volcanism in Central America: 2. Tephra volumes and erupted masses. *Geochemistry, Geophysics, Geosystems*, 9, Q02502. <https://doi.org/10.1029/2007GC001791>
- Kutterolf, S., Freundt, A., Pérez, W., Wehrmann, H., & Schmincke, H.-U. (2007). Late Pleistocene to Holocene temporal succession and magnitudes of highly-explosive volcanic eruptions in West-Central Nicaragua. *Journal of Volcanology and Geothermal Research*, 163(1–4), 55–82.
- Laiolo, M., Coppola, D., Barahona, F., Benítez, J. E., Cigolini, C., Escobar, D., et al. (2017). Evidences of volcanic unrest on high-temperature fumaroles by satellite thermal monitoring: The case of Santa Ana volcano, El Salvador. *Journal of Volcanology and Geothermal Research*, 340, 170–179. <https://doi.org/10.1016/j.jvolgeores.2017.04.013>
- Lesne, P., Kohn, S. C., Blundy, J., Witham, F., Botcharnikov, R. E., & Behrens, H. (2011). Experimental simulation of closed-system degassing in the system basalt-H₂O-CO₂-S-Cl. *Journal of Petrology*, 52(9), 1737–1762.
- Longpré, M. A., Stix, J., Costa, F., Espinoza, E., & Muñoz, A. (2014). Magmatic processes and associated timescales leading to the January 1835 eruption of Cosigüina volcano, Nicaragua. *Journal of Petrology*, 55(6), 1173–1201.
- Martin, R. S., Sawyer, G. M., Spampinato, L., Salerno, G. G., Ramirez, C., Ilyinskaya, E., et al. (2010). A total volatile inventory for Masaya volcano, Nicaragua. *Journal of Geophysical Research*, 115, B09215. <https://doi.org/10.1029/2010JB007480>
- Mather, T. A., Pyle, D. M., Tsanev, V. I., McGonigle, A. J. S., Oppenheimer, C., & Allen, A. G. (2006). A reassessment of current volcanic emissions from the Central American arc with specific examples from Nicaragua. *Journal of Volcanology and Geothermal Research*, 149(3–4), 297–311.
- Mavrogenes, J. A., & O'Neill, H. S. C. (1999). The relative effects of pressure, temperature and oxygen fugacity on the solubility of sulfide in mafic magmas. *Geochimica et Cosmochimica Acta*, 63(7–8), 1173–1180.
- McBirney, A. R. (1956). The Nicaraguan volcano Masaya and its caldera. *Transactions of the American Geophysical Union*, 37(1), 83–96.
- Moretti, R., & Baker, D. R. (2008). Modeling the interplay of fO₂ and fS₂ along the FeS-silicate melt equilibrium. *Chemical Geology*, 256, 285–297.
- Moretti, R., & Papale, P. (2004). On the oxidation state and volatile behaviour in multicomponent gas–melt equilibria. *Chemical Geology*, 213(1–3), 265–280. <https://doi.org/10.1016/j.chemgeo.2004.08.048>
- Moretti, R., Papale, P., & Ottonello, G. (2003). A model for the saturation of C-O-H-S fluids in silicate melts, in *Volcanic degassing. Geological Society London, Special Publication*, 213(1), 81–101.
- Moune, S., Gauthier, P.-J., & Delmelle, P. (2010). Trace elements in the particulate phase of the plume of Masaya volcano, Nicaragua. *Journal of Volcanology and Geothermal Research*, 193(3–4), 232–244.
- Moune, S., Holtz, F., & Botcharnikov, R. E. (2009). Sulphur solubility in andesitic to basaltic melts: Implications for Hekla volcano, Cotrib. *Mineralogy and Petrology*, 157(6), 691–707.
- Nadeau, P. A., & Williams-Jones, G. (2009). Apparent downwind depletion of volcanic SO₂ flux—Lessons from Masaya volcano, Nicaragua. *Bulletin of Volcanology*, 71(4), 389–400.
- Oppenheimer, C., Lomakina, A. S., Kyle, P. R., Kingsbury, N. G., & Boichu, M. (2009). Pulsatory magma supply to a phonolite lava lake. *Earth and Planetary Science Letters*, 284(3–4), 392–398.
- Oppenheimer, C., McGonigle, A. J. S., Allard, P., Wooster, M. J., & Tsanev, V. (2004). Sulfur, heat, and magma budget of Erta 'Ale lava lake, Ethiopia. *Geology*, 32(6), 509–512.
- Palma, J. L., Calder, E. S., Basualto, D., Blake, S., & Rothery, D. A. (2008). Correlations between SO₂ flux, seismicity, and outgassing activity at the open vent of Villarrica volcano, Chile. *Journal of Geophysical Research*, 113, B10201. <https://doi.org/10.1029/2008JB005577>
- Patrick, M., Orr, T., Sutton, A. J., Elias, T., & Swanson, D. (2013). *The first five years of Kilauea's summit eruption in Halema'uma'u crater, 2008–2013* (Fact Sheet 2013–3116). Reston, VA: U.S. Geological Survey. <https://doi.org/10.3133/fs2013116>
- Patrick, M. R., Orr, T., Sutton, A. J., Lev, E., Thelen, W., & Fee, D. (2016). Shallowly driven fluctuations in lava lake outgassing, Kilauea Volcano, Hawaii. *Earth and Planetary Science Letters*, 433, 326–338.
- Pearson, S. C. P., Kiyosugi, K., Lehto, H. L., Saballos, J. A., Connor, C. B., & Sanford, W. E. (2012). Integrated geophysical and hydrothermal models of flank degassing and fluid flow at Masaya volcano, Nicaragua. *Geochemistry, Geophysics, Geosystems*, 13, Q05011. <https://doi.org/10.1029/2012GC004117>
- Pérez, W., & Freundt, A. (2006). The youngest highly explosive basaltic eruptions from Masaya Caldera (Nicaragua). In W. I. Rose et al. (Eds.), *Volcanic Hazards in Central America, Geological Society of America Special Papers* (Vol. 412, pp. 189–207).
- Pérez, W., Freundt, A., Kutterolf, S., & Schmincke, H.-U. (2009). The Masaya Triple Layer: A 2100 year old basaltic multi-episodic Plinian eruption from the Masaya Caldera Complex (Nicaragua). *Journal of Volcanology and Geothermal Research*, 179(3–4), 191–205.
- Platt, U., & Stutz, J. (2008). *Differential optical absorption spectroscopy: Principles and applications, physics of earth and space environments*. Berlin, Germany: Springer. https://doi.org/10.1007/978-3-540-75776-4_2
- Portnyagin, M. V., Hoernle, K., & Mironov, N. L. (2014). Contrasting compositional trends of rocks and olivine-hosted melt inclusions from Cerro Negro volcano (Central America): Implications for decompression-driven fractionation of hydrous magmas. *International Journal of Earth Sciences*, 103(7), 1963–1982.
- Putirka, K. D., (2008). Thermometers and barometers for volcanic systems. In K. D. Putirka & F. J. Tepley (Eds.), *Minerals, inclusions and volcanic processes* (pp. 61–120). Chantilly, VA: Mineralogical Society of America.
- Robidoux, P., Aiuppa, A., Rotolo, S., Rizzo, A. L., & Hauri, E. H. (2017a). The volatile content of mafic-to-intermediate magmas from San Cristóbal volcano, Nicaragua. *Lithos*, 272–273, 147–163.
- Robidoux, P., Rotolo, S. G., Aiuppa, A., Lanzò, G., & Hauri, E. H. (2017). Geochemistry and volatile content of magmas feeding explosive eruptions at Telica volcano (Nicaragua). *Journal of Volcanology and Geothermal Research*, 341, 131–148. <https://doi.org/10.1016/j.jvolgeores.2017.05.007>
- Roggensack, K., Hervig, R. L., McKnight, S. B., & Williams, S. N. (1997). Explosive basaltic volcanism from Cerro Negro: Influence of volatiles on eruptive style. *Science*, 277(5332), 1639–1642.
- Rothery, D. A., Coppola, D., & Saunders, C. (2005). Analysis of volcanic activity patterns using MODIS thermal alerts. *Bulletin of Volcanology*, 67(6), 539–556.
- Rymer, H., Van Wyk De Vries, B., Stix, J., & Williams-Jones, G. (1998). Pit crater structure and processes governing persistent activity at Masaya volcano, Nicaragua. *Bulletin of Volcanology*, 59(5), 345–355.

- Sadofsky, S. J., Portnyagin, M. V., Hoernle, K., & van den Bogaard, P. (2008). Subduction cycling of volatiles and trace elements through the Central American volcanic arc: Evidence from melt inclusions. *Contributions to Mineralogy and Petrology*, 155(4), 433–456. <https://doi.org/10.1007/s00410-007-0251-3>
- Shinohara, H. (2008). Excess degassing from volcanoes and its role on eruptive and intrusive activity. *Reviews of Geophysics*, 46, RG4005. <https://doi.org/10.1029/2007RG000244>
- Shinohara, H., Aiuppa, A., Giudice, G., Gurrieri, S., & Liuzzo, M. (2008). Variation of H₂O/CO₂ and CO₂/SO₂ ratios of volcanic gases discharged by continuous degassing of Mount Etna volcano, Italy. *Journal of Geophysical Research*, 113, B09203. <https://doi.org/10.1029/2007JB005185>
- Spampinato, L., Ganci, G., Hernández, P. A., Calvo, D., Tedesco, D., Pérez, N. M., et al. (2013). Thermal insights into the dynamics of Nyiragongo lava lake from ground and satellite measurements. *Journal of Geophysical Research: Solid Earth*, 118, 5771–5784. <https://doi.org/10.1002/2013JB010520>
- Stephens, K., Biggs, J., Ebmeier, S., Young, N., & Wauthier, C. (2017). *Uncovering the mysteries behind lava lake deformation source mechanisms: A case study of the ephemeral lava lake at Masaya volcano, Nicaragua*. Abstract #652 presented at Proceedings of the IAVCEI 2017 Conference, Portland, OR, August 2017.
- Stevenson, D. S., & Blake, S. (1998). Modelling the dynamics and thermodynamics of volcanic degassing. *Bulletin of Volcanology*, 60(4), 307–317. <https://doi.org/10.1007/s004450050234>
- Stix, J. (2007). Stability and instability of quiescently active volcanoes: The case of Masaya, Nicaragua. *Geology*, 35(6), 535–538.
- Stoiber, R. E., Williams, S. N., & Huebert, B. J. (1986). Sulfur and halogen gases at Masaya caldera complex, Nicaragua: Total flux and variations with time. *Journal of Geophysical Research*, 91(B12), 12215–12231.
- Tamburello, G. (2015). Ratiocalc: Software for processing data from multicomponent volcanic gas analyzers. *Computers & Geosciences*, 82, 63–67.
- Van Wyk de Vries, B. (1993). *Tectonics and magma evolution of Nicaraguan volcanic systems* (PhD thesis). Milton Keynes, UK: Open University.
- Vergnolle, S., & Bouche, E. (2016). Gas-driven lava lake fluctuations at Erta 'Ale volcano (Ethiopia) revealed by MODIS measurements. *Bulletin of Volcanology*, 78(9), 1–28.
- Walker, J. A., Williams, S. N., Kalamarides, R. I., & Feigenson, M. D. (1993). Shallow open-system evolution of basaltic magma beneath a subduction zone volcano—The Masaya Caldera Complex, Nicaragua. *Journal of Volcanology and Geothermal Research*, 56(4), 379–400.
- Wallace, P. J. (2005). Volatiles in subduction zone magmas: Concentrations and fluxes based on melt inclusions and volcanic gas data. *Journal of Volcanology and Geothermal Research*, 140(1–3), 217–240.
- Wallace, P. J., Plank, Edmonds, T. M., & Hauri, E. H. (2015). Volatiles in Magmas. In H. Sigurdsson, B. Houghton, S. McNutt, H. Rymer, & J. Stix (Eds.), *The encyclopedia of volcanoes* (2nd ed., pp. 163–183). Cambridge, MA: Academic Press.
- Wehrmann, H., Hoernle, K., Portnyagin, M., Wiedenbeck, M., & Heydolph, K. (2011). Volcanic CO₂ output at the Central American subduction zone inferred from melt inclusions in olivine crystals from mafic tephros. *Geochemistry, Geophysics, Geosystems*, 12, Q06003. <https://doi.org/10.1029/2010GC003412>
- Werner, C., Kern, C., Coppola, D., Lyons, J. J., Kelly, P. J., Wallace, K. L., et al. (2017). Magmatic degassing, lava dome extrusion, and explosions from Mount Cleveland volcano, Alaska, 2011–2015: Insight into the continuous nature of volcanic activity over multi-year time-scales. *Journal of Volcanology and Geothermal Research*, 337, 98–110.
- Williams, S. N. (1983). Plinian airfall deposits of basaltic composition. *Geology*, 11, 211–214.
- Williams-Jones, G., Rymer, H., & Rothery, D. A. (2003). Gravity changes and passive SO₂ degassing at the Masaya caldera complex, Nicaragua. *Journal of Volcanology and Geothermal Research*, 123(1–2), 137–160.
- Witter, J. B., Victor, C., Kress, P., Delmelle, J., & Stix, J. (2004). Volatile degassing, petrology, and magma dynamics of the Villarrica lava lake, Southern Chile. *Journal of Volcanology and Geothermal Research*, 134(4), 303–337.
- Wooster, M. J., Zhukov, B., & Oertel, D. (2003). Fire radiative energy for quantitative study of biomass burning: Derivation from the BIRD experimental satellite and comparison to MODIS fire products. *Remote Sensing of Environment*, 86(1), 83–107.
- Wright, R., Flynn, L., Garbeil, H., Harris, A. J. L., & Pilger, E. (2002). Automated volcanic eruption detection using MODIS. *Remote Sensing of Environment*, 82(1), 135–155.
- Wright, R., Flynn, L. P., Garbeil, H., Harris, A. J. L., & Pilger, E. (2004). MODVOLC: Near-real-time thermal monitoring of global volcanism. *Journal of Volcanology and Geothermal Research*, 135(1–2), 29–49.
- Wright, R., Garbeil, H., & Harris, A. J. L. (2008). Using infrared satellite data to drive a thermo-rheological/stochastic lava flow emplacement model: A method for near-real-time volcanic hazard assessment. *Geophysical Research Letters*, 35, L19307. <https://doi.org/10.1029/2008GL035228>
- Zurek, J. M. (2016). *Multidisciplinary investigation of the evolution of persistently active basaltic volcanoes* (PhD thesis). Burnaby, BC, Canada: Simon Fraser University.